ABSTRACT

GAY, ALEX MICHAEL. Fabrication and Classification of Dual-Matrix Composites for Deployable Space Applications (Under the direction of Dr. Mark Pankow).

High strain composites (HSCs) are materials capable of large deformations, but they also have high stiffness which allows them to reconfigure and carry loads. As such they are of interest for deployable space structures. HSCs aim to reduce the weight, cost, and complexity of deployable space structures by replacing traditional metallic structures and mechanical hinges. Dual-matrix composites are a subset of HSCs that utilize the high flexibility of carbon fiber reinforced silicone (CFRS) alongside a stiffer epoxy matrix to create localized flexible hinge regions within a thin carbon fiber composite. Intrinsic hinges allow for fabrication of origami dual-matrix composites that present an interesting opportunity for space structures; the folding arrangements that can be achieved allow for highly efficient packing and produce structures capable of self-deployment. Origami folding techniques can be used to create flat folding deployable structures and mechanical metamaterials which can then be applied to dual-matrix composites. However, their manufacture is not well-established thus fabrication of dual-matrix composites presents a challenge. Accessible out-of-autoclave methods of dual-matrix composite fabrication are explored. A computer numerical control (CNC) plotter is developed to accurately and consistently infuse silicone into complex origami hinge architectures. Dual-matrix composite samples were tested to characterize the response to extreme bending.

Fabrication and Classification of Dual-Matrix Composites for Deployable Space Applications

by
Alex Michael Gay

A thesis submitted to the Graduate Faculty of
North Carolina State University
in partial fulfillment of the
requirements for the degree of
Master of Science

Aerospace Engineering

Raleigh, North Carolina

2017

APPROVED BY:

_____	_____
Dr. Andre Mazzoleni	Dr. Philip Bradford

_____

Dr. Mark Pankow

Committee Chair

DEDICATION

Mom and Dad, thanks for providing me with every opportunity to succeed and encouraging to chase my dreams.

BIOGRAPHY

Alex Gay received his Bachelor of Science degree in Materials Science and Engineering from Clemson University in May 2015. His desire to contribute to the space industry led him to North Carolina State University where he began work on his Master of Science in Aerospace Engineering that fall. He began his work with Dr. Mark Pankow fabricating dual-matrix origami composite structures for use in deployable space structure applications. Over the summer of 2016 Alex had the opportunity to intern at NASA Langley Research Center in Hampton, VA where he continued working with flexible carbon fiber composites for deployable space structure applications.

ACKNOWLEDGMENTS

First and foremost, I would like to thank my advising professor Dr. Mark Pankow for providing me the opportunity to fabricate and explore unique composite materials in the great environment that is the BLAST Lab. Not many people have the opportunity to build a carbon fiber origami crane, let alone a robotic assistant to help them do it again.

Charlie, thanks for all the help you provided me from composite fabrication to machining stuff to help with my projects. Cody, thanks for all the help with the printer and everything else under the ceiling. Jordan, thanks for all the knowledge, composites and otherwise, you provided. John and Tyler, thanks for all the work you guys put in to help get the printer up and running. Thanks to everyone else in the BLAST Lab, you guys have all helped me out in some way or another and have been great to work with these last couple years. Finally, Leo, I appreciate you sticking with me through it all.

TABLE OF CONTENTS

LIST OF TABLES

LIST OF FIGURES

Chapter 1 – Introduction

1.1 – Background

Current technology requires that structures for space missions fit inside the cargo volume of their launch vehicle. Unfortunately, many space missions necessitate large structures. The volumetric constraints imposed by launch capabilities have been addressed in the past by utilizing deployable capabilities and structural modularity. These allow for payloads to expand to many times their packaged size or be assembled further in space, respectively. Development of efficient packing technologies is critical to sending larger structures into space without requiring larger and more expensive launch vehicles. This study examines fiber reinforced composites able to undergo large strains that are capable of ushering in the next generation of deployable space structures.

Traditional deployable space structures utilize mechanical hinges to expand from their packaged state. While the performance of mechanical hinges is well understood, they present their own challenges in the form of moving parts and high mass. Reducing the total moving parts within a space mission is ideal since each moving part is a potential point of failure and cannot easily be serviced after launch. The hinges add cost and mass because of the high precision demanded and interface surfaces required [1]. Other deploying space structures have been tested that weld the structure as it deploys [2], but this prevents reconfiguring of the structure after deployment if necessary. High strain composites (HSCs) have the capacity to mitigate these issues by taking the place of metallic, mechanical solutions with more lightweight, monolithic elements.

High strain composites are materials capable of large deformations, but they also have high stiffness which allows them to reconfigure and carry loads. The mechanics of stiff fibers within a softer matrix allow HSCs to achieve large strains without phase transformations like those seen in superelastic metallic alloys. The processes that allow such deformations are reversible which allows HSCs to be strained and released repeatedly. The dependency of the properties of HSCs on their structural configuration allows for applications that could not be realized with other materials. HSCs using fiberglass were developed around the same time as

metallic high strain deploying structures and have flown on numerous spaceflight missions, but when comparing material properties to those of the metallic alternatives, glass fiber reinforced composite structures offered no advantage over their metal cousins so there was not much interest. In recent years, however, this has changed as improved carbon fiber technologies have allowed for strong, light, and thermally stable composites, allowing for technological solutions capable of surpassing those achieved using rigid, metallic deploying structures [3].

Numerous designs that take advantage of HSCs have been realized for deployable space applications. One well-known example is the omega cross-section boom developed by the German Aerospace Center (DLR) for use on solar sail deployment. The boom is made of two omega shaped carbon fiber shells joined together to form a closed cross section as seen in Figure 1. The extremely small thickness of the material allows the boom to flatten without damaging the fibers or matrix. The flattening ability and flexibility gives the boom the ability to be rolled around a central circular hub and packed into a small volume. Upon deployment, the boom returns to its fabricated omega shape and regains its stiffness along its length [4].

Developments have also been made on hinged booms with sections capable of folding to allow compact packing for launch and deployment in space. A section of a circular cross-section boom is cut out to form a tape-spring hinge that is able to bend while the rest of the boom remains rigid. The hinge region can be flattened and folded to allow the boom to be

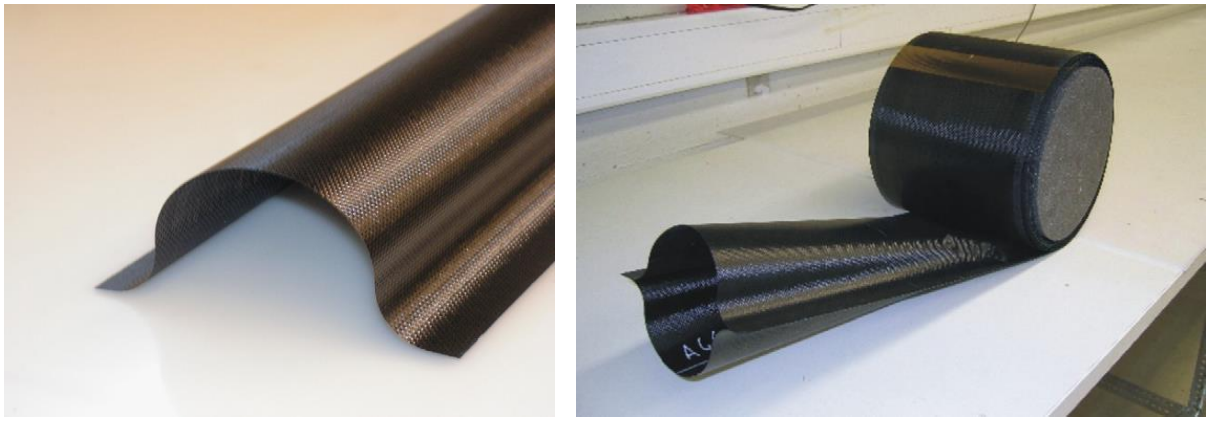

FIGURE 1. DLR'S OMEGA BOOM HALF-SHELL AND COILED FULL BOOM [4]

packed in a compact configuration, see Figure 2. Since the energy is stored using linear elastic strain the boom can self-deploy once released [5].

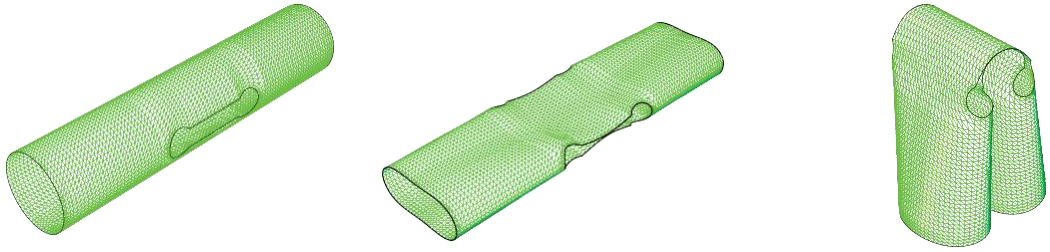

FIGURE 2. TAPE-SPRING HINGE INITIAL CONFIGURATION, FLATTENED, AND FOLDED [5]

The examples discussed up to this point have all used a relatively stiff polymer matrix material. Although the fibers are much stiffer than the matrix material, there is also the option of utilizing a hyperelastic matrix material to allow even more extreme deformations of the composite. By infusing the carbon fibers with a material such as a silicone rubber, the thin composites can be folded without damaging the fibers. The soft matrix allows the fibers to move and experience microbuckling when the composite is in bending which prevents the inherently brittle fibers from breaking, see Figure 3 [6]. These extreme folding capabilities present opportunities for new developments in highly packable structures.

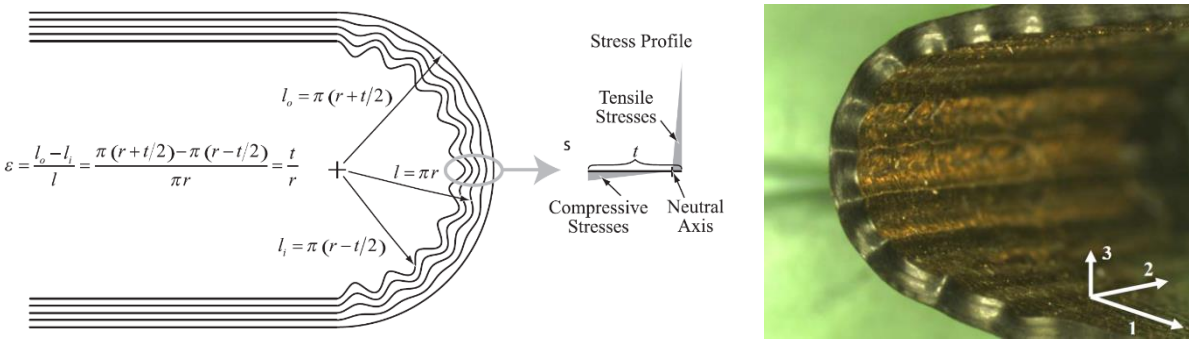

FIGURE 3. FIBER MICROBUCKLING IN A SOFT-MATRIX COMPOSITE [6]

One such example of a structure that has taken advantage of the great flexibility of carbon fiber reinforced silicone (CFRS) is a deployable umbrella type reflector. This particular reflector design utilizes a triaxial woven carbon fiber to reinforce a silicone matrix and is highly applicable to satellites because of its ability to deploy a large dish from a small package, see Figure 4. The geometry of the reflecting surface is highly accurate and dimensionally stable

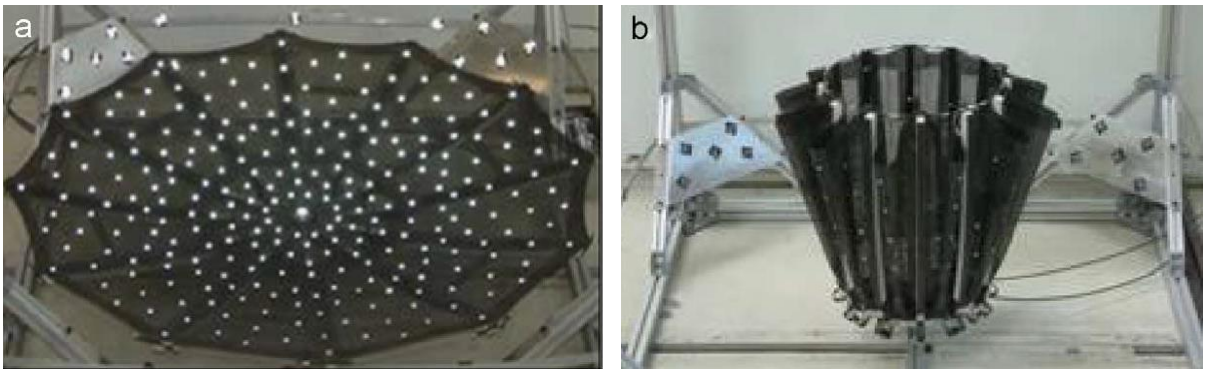

FIGURE 4. CARBON FIBER REINFORCED SILICONE (CFRS) REFLECTING SURFACE IN DEPLOYED AND FOLDED STATES [7]

with a very low mass. The design parameters of the reflecting surface can be modified depending on the frequencies to be gathered by the reflector [7].

Dual-matrix composites are a subset of high strain composites that utilize the high flexibility of CFRS alongside a stiffer epoxy matrix to create localized flexible hinge regions within a thin carbon fiber composite. The independence of the two matrix regimes results in a relatively stiff composite with an epoxy matrix and a much softer and more flexible composite with a silicone matrix. This allows for intrinsic hinges within a continuous deployable composite structure as seen in Figure 5 [8].

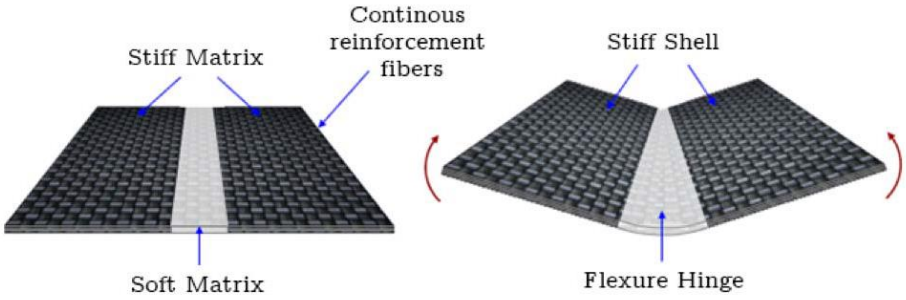

FIGURE 5. FLEXIBLE DUAL-MATRIX COMPOSITE SCHEMATIC DIAGRAM [9]

Dual-matrix composites have garnered significant interest with regard to deployable space structures for their low mass and extremely high packing efficiency. The localized folding regions allow for deliberate and intricate folding patterns to be realized. Folding techniques have been applied to dual-matrix composites to create highly packable deployable structures. One such application is a deployable conical antenna developed for use aboard

CubeSat missions. The conical composite shell contains an embedded conductive element for the antenna structure. The composite shell is able to be flattened then Z-folded for further compaction as seen in Figure 6 [10]. Other dual-matrix composite concepts that have been investigated for space applications include foldable booms [9], beams containing flexible hinges [11], and origami structures [3].

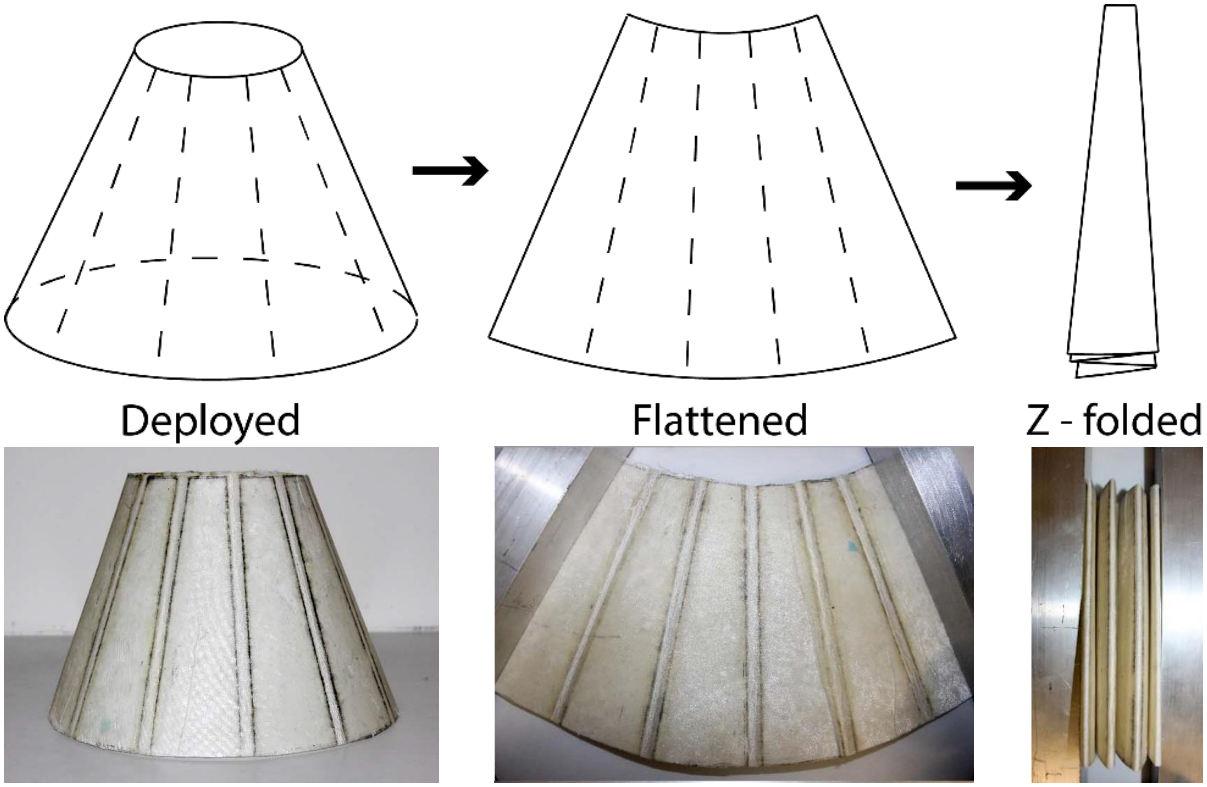

FIGURE 6. FOLDING PROCESS OF CONICAL DUAL-MATRIX COMPOSITE ANTENNA [10]

Origami dual-matrix composites present an interesting opportunity for space structures because the folding techniques that can be realized allow for highly efficient packing and produce structures capable of self-deployment. Substituting classical origami's paper with high-performance materials like fiberglass and carbon fiber dual-matrix composites produces structures with flexible regions capable of emulating an origami fold and very rigid regions elsewhere capable of supporting significant loads. This combination of stiffness and flexibility results in structures that can pack tightly but still serve as structural elements for a potential space mission and deploy to sizes much larger than their packaged configuration.

It has been shown that high strain and dual-matrix composites present the opportunity to remove the need for heavy and expensive complex mechanical hinges from deployable structures. These materials provide new methods of packaging and deploying structures aboard payloads constrained by the volumetric limitations of spacecraft. However, their manufacture is not well-established thus fabrication of dual-matrix composites presents a challenge. Fabrication of dual-matrix composites by hand often results in hinge inconsistencies and geometric flaws and is very time consuming, resulting in costly downtime. The issues of dual-matrix composite fabrication need to be ironed out before they can be regularly implemented into spaceflight missions.

1.2 – Research Objectives

Fabrication methods of dual-matrix composites will be investigated to expand understanding of accessible and out-of-autoclave techniques. A novel computer numerical controlled (CNC) method of dual-matrix composite fabrication will be explored and developed to increase accuracy and consistency of hinge regions to the level demanded by complex origami layouts. Dual-matrix composites will be manufactured using origami techniques to create deployable structures. Comparisons will be made between hand fabricated dual-matrix composites and those made using the CNC method. Dual-matrix laminates will be experimentally tested using new test methods to accurately characterize bending stiffness of coupon samples.

1.3 – Research Questions

- How can fabrication of dual-matrix composites be made more reliable to consistently attain the accuracy demanded by origami folds?
- How can origami folding of flexible composites be integrated into deployable structures for space applications?
- How can dual-matrix composites subjected to extreme bending be characterized and what kind of mechanical properties can be extracted?

1.4 – Thesis Outline

Chapter 2 will investigate origami folding techniques to create deployable structures capable of efficient packing that can be applied to complex dual-matrix composite architectures. Chapter 3 will explore methods of fabricating dual-matrix by hand, examine some of the challenges presented in doing so, and provide the basis for the development of a CNC device to assist in manufacture of dual-matrix composites. Chapter 4 will detail the development of a CNC 'printer' for producing more consistent silicone geometries infused into a carbon fiber fabric and the outcomes of that endeavor. Chapter 5 will investigate an empirical test method to characterize highly flexible composite materials under extreme bending. Chapter 6 will conclude this study and provide direction for future work.

Chapter 2 – Complex Origami Structures

This chapter will explore the field of origami engineering in which inspiration is drawn from traditional origami folding techniques to devise folding and morphing structures. These folding structures are of interest because the ability to integrate specific, localized hinge regions of extreme flexibility allows dual-matrix composites to adapt origami concepts to produce structures using high-performance composite materials that can be used aboard space-faring missions.

2.1 – Origami Engineering

Origami is the traditional Japanese art of folding a flat piece paper into three-dimensional shapes and figures. Traditionally, origami is used to create decorative pieces, but by adapting traditional folding techniques, it is possible to create practical structures. Origami folding techniques provide inspiration for new developments of adaptive, morphing, and small-packing structures. NASA's Pop-Up Flat Folding Explorer Robot (PUFFER), seen in Figure 7, is an example of an origami-inspired engineering design. The robotic explorer is designed as a small companion to rovers that can explore areas that may be unfavorable for the larger rover. The PUFFER's wheels fold inward such that the robot can almost completely flatten

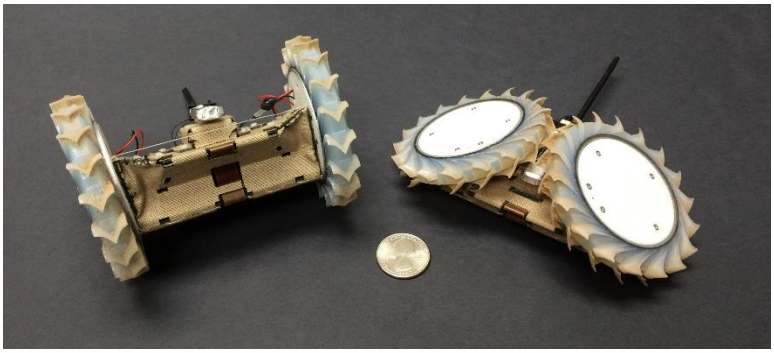

FIGURE 7. PUFFER IN STANDARD AND FLATTENED CONFIGURATIONS [12]

itself, allowing for exploration of low vertical clearance areas and efficient packing so one or more explorers can be easily carried aboard the rover itself [12]. While the PUFFER uses an origami-inspired design, other recently developed technologies incorporate origami folds as

part of their structure. NASA and Brigham Young University (BYU) have explored active radiator concepts for satellites that can be seen in Figure 8. The radiators use their origami architectures to change shape; the resulting changes in depth of the cavities controls the heat loss of the radiators [13]. One of the major stimuli of interest in origami engineering was the

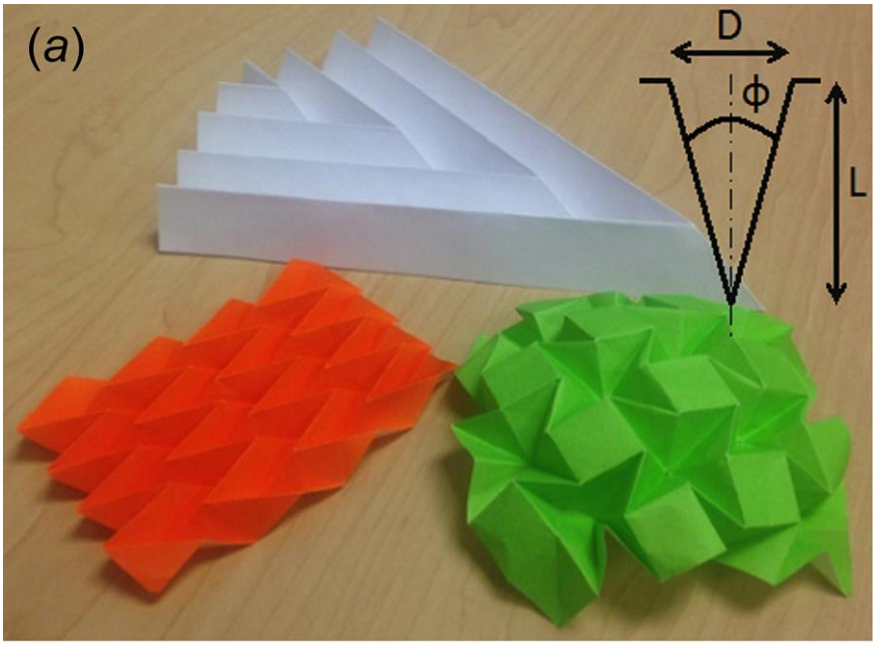

FIGURE 8. POTENTIAL ORIGAMI MORPHING RADIATOR DESIGNS [13]

Miura folded solar array that flew on the Japanese Space Flyer Unit in 1995 [14], [15]. The structure introduced by Miura folding exhibits a memory effect that allows it to be easily opened and closed [16]. Since then, researchers at BYU have explored further concepts for self-deploying, highly packable solar arrays. A modified 'flasher' model was developed that allowed rigid solar cell elements to be rolled up compactly without damaging the cells, see Figure 9 [17]. It has been shown that this concept can be adapted to and replicated using dual-matrix composite materials as seen in Figure 10 [18].

FIGURE 9. DEPLOYMENT OF MODIFIED FLASHER DEPLOYABLE SOLAR ARRAY CONCEPT [17]

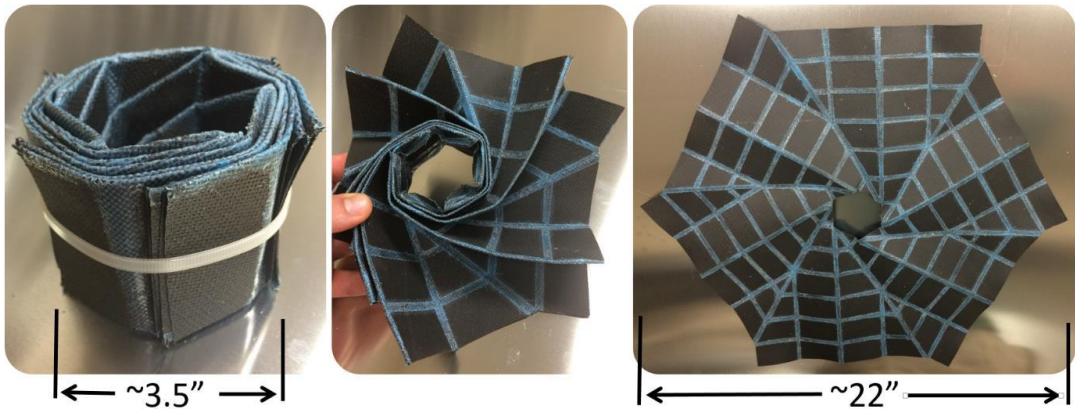

FIGURE 10. DEPLOYMENT OF CARBON FIBER DUAL-MATRIX MODIFIED FLASHER MODEL [18]

2.1 – Origami Mechanical Metamaterials

In the context of this work, mechanical metamaterials refer to materials with properties primarily determined by the geometric configuration of the material. The Miura folding technique provides a versatile basis capable of being adapted to metamaterials. A partially folded Miura-folded sheet on its own is a simple shell metamaterial; the localized fold pattern alters the bulk mechanical properties, most notably, the Miura sheet has a negative in-plane Poisson’s ratio. By stacking Miura sheets of slightly different geometries, a 3D, folding cellular metamaterial structure is created, as seen in Figure 11. Such structures can be tailored to automatically arrest folding by incorporating alterations of the Miura unit cell within layers depending on the desired amount of folding [19].

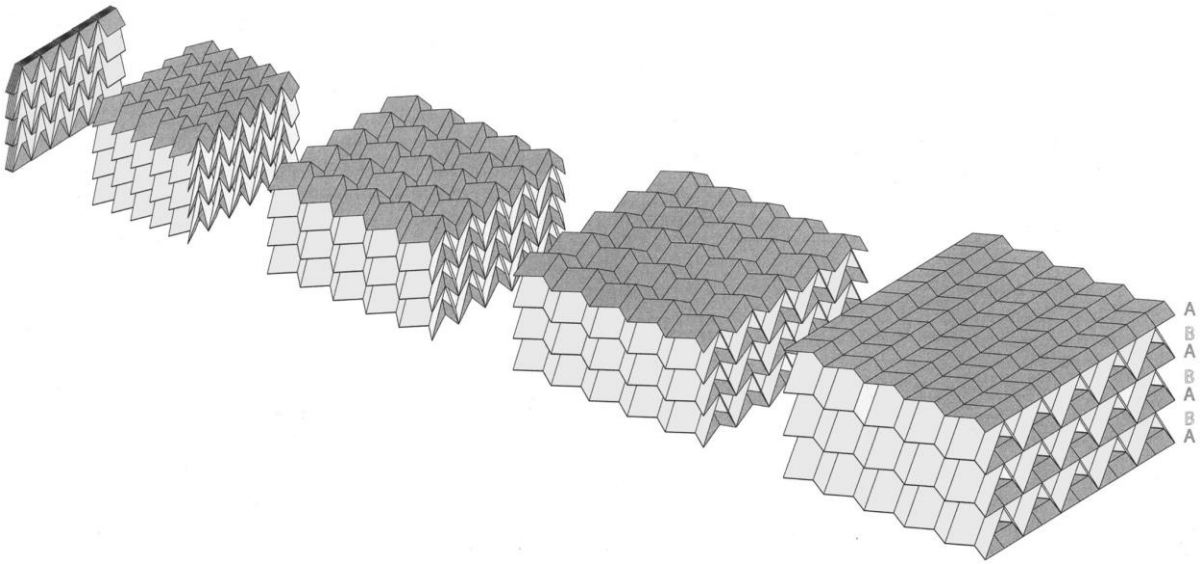

FIGURE 11. 3D FOLDING MIURA CELLULAR METAMATERIAL [19]

Other cellular metamaterial structures have been developed that exhibit highly anisotropic behaviors. The structure shown in Figure 12 is foldable along its *x* and y axes but rigid in the *z* direction. By isolating the Miura pattern segments within the structure, it is possible to fabricate the cellular metamaterials in a flat configuration to later be expanded into its 3D configuration [20].

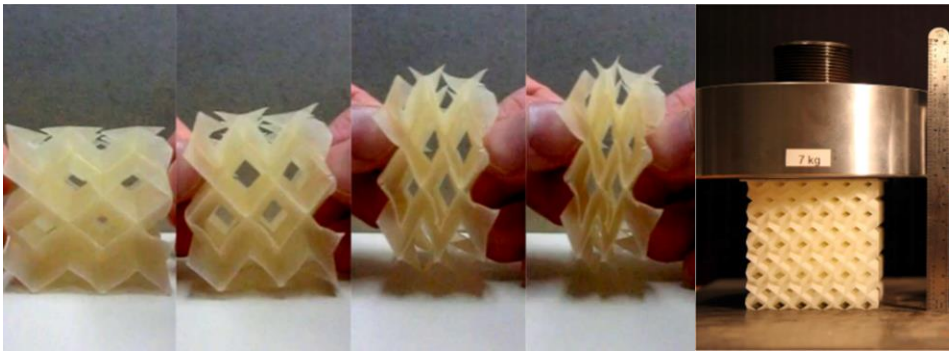

FIGURE 12. 3D CELLULAR ORIGAMI METAMATERIAL WITH SINGLE-AXIS RIGIDITY [20]

By combining elements from a Miura sheet it is possible to make flattening and flat-folding tubes. The tube is created when a row of Miura cells is joined along the edges with its mirror image. When fully extended, the tube lies flat in its *XY* plane and when fully retracted it folds flat in its *YZ* plane; both the fabrication and extension/retraction can be seen in Figure

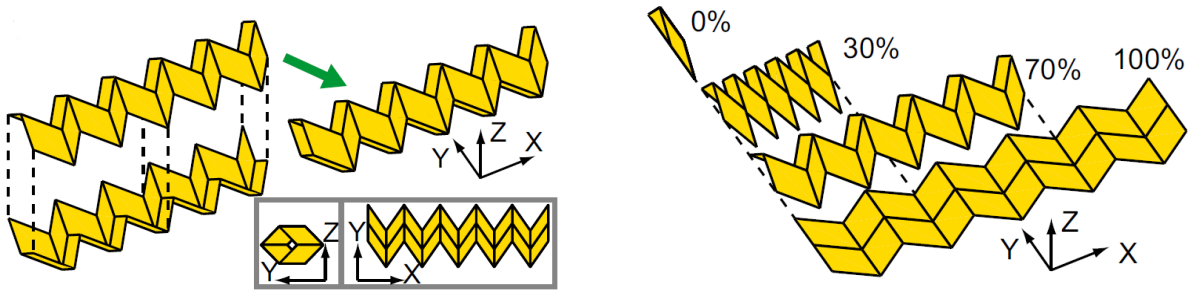

FIGURE 13. FABRICATION OF MIURA TUBE AND EXTENSION/RETRACTION MECHANISM [21]

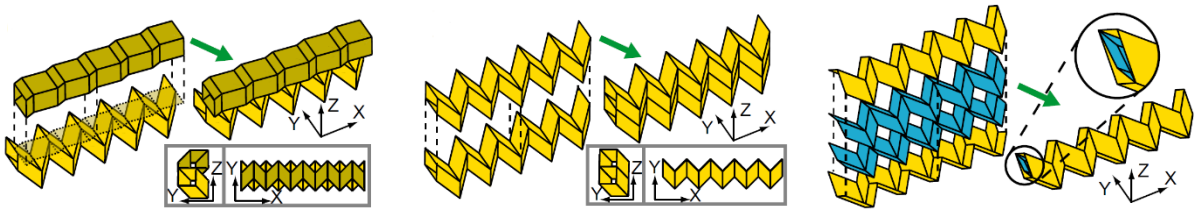

FIGURE 14. ZIPPER-, ALIGNED-, AND INTERNALLY-COUPLED MIURA TUBE CONFIGURATIONS [21]

13. The tubes can be coupled with another in different configurations to bolster the mechanical properties. Three different configurations can be seen in Figure 14. The zipper-configured tubes are stiffer than the other two configurations and the only ones to retain the flattening characteristics. The tubes can be further assembled into larger cellular structures that maintain a degree of flattening and deployability. Deployable structures that have been fabricated include an architectural canopy and a bridge; both can be seen in Figure 15. Both the canopy and bridge have a high out-of-plane stiffness and are capable of supporting such loads. These designs present opportunities for future developments in origami-inspired architecture [21].

The concepts presented above can be applied to dual-matrix composites by infusing silicone into the locations of the origami fold lines creating flexible folding regions and stiff panels elsewhere. The carbon fiber reinforcement provides a stiffer structure than paper while being lighter than metallic solutions, and it is also continuous throughout the origami structure unlike other materials that would require a discrete hinge. The ability to manufacture these origami metamaterials using carbon fiber would produce lightweight, high-performance

deployable structures. The promise of such structures drives the need for accessible methods of manufacturing the dual-matrix composite materials involved.

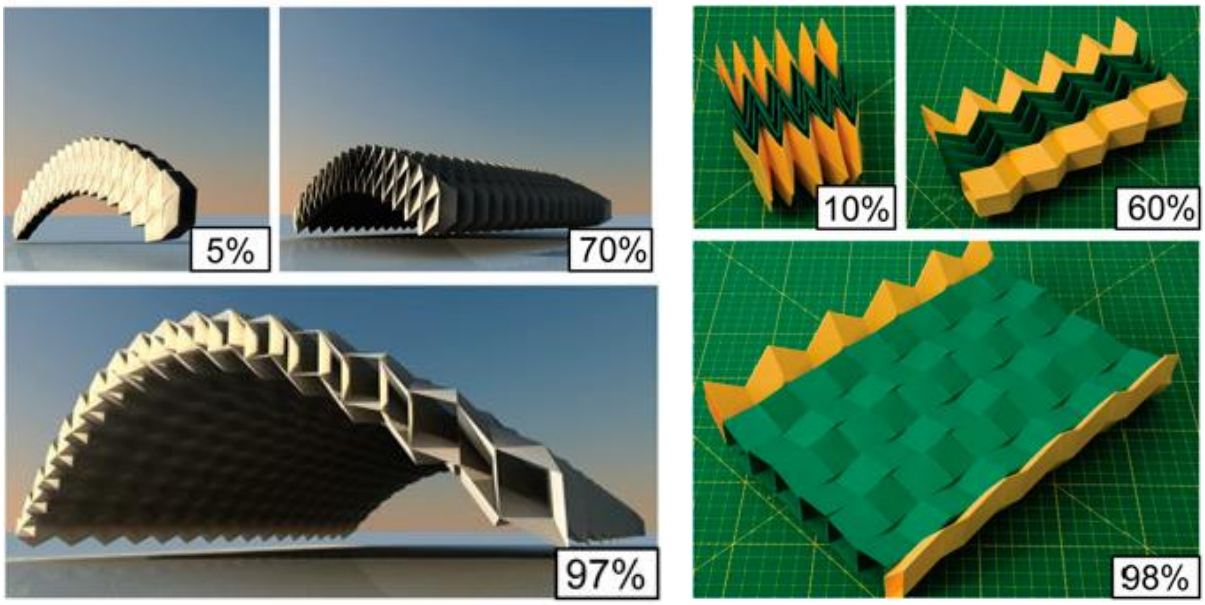

FIGURE 15. CANOPY AND BRIDGE STRUCTURES CREATED USING MIURA TUBES IN VARIOUS STATES OF DEPLOYMENT [21]

Chapter 3 – Hand Fabrication of Dual-Matrix Composites

This chapter will discuss the materials involved in the fabrication of dual-matrix composites and the methods of fabricating complex folding architectures with integral hinges. Dual-matrix composite origami are fabricated and folded. The challenges presented by hand fabrication of dual-matrix composites are discussed, and the inspirations for devising a CNC plotter to infuse silicone hinge regions are laid out.

3.1 – Materials

The materials used within this study were primarily selected for convenience; the techniques used can easily be applied to different material systems depending on the desired properties of the final composite parts. For spacefaring composites, for example, it is crucial that the materials involved do not outgas under vacuum lest they release anything that might adversely affect other elements of the payload. As long as all the material systems within the composite are compatible, substitutions can be freely made to tune the mechanical properties of the finished product or the fabrication parameters, such as cure times or mechanisms.

The fiber reinforcement used in the fabrication of dual-matrix composites in this study was primarily a 3k plain-woven carbon fiber fabric. The 3k fabric offers a balance between rigidity of the stiff regions and overall fabric thinness. The epoxy resin system used for the stiff regions is Fibre Glast's 2000 series with 2060 hardener, which results in a one hour pot life. The epoxy resin system reaches full cure after 36 hours. Two different two-part silicone rubber systems were tested for use in the flexible hinge regions: Smooth-On Mold Star 30 and Smooth-On Smooth-Sil 950. Both silicone rubber systems have a 45 minute pot life; the Mold Star 30 cures in 6 hours while the Smooth-Sil 950 takes 24 hours. The relevant mechanical properties of each matrix system can be seen in Table 1.

TABLE 1. MECHANICAL PROPERTIES OF MATRIX SYSTEMS

Matrix System	*Modulus [psi]*	*Elongation [%]*	*Viscosity [cps]*	*Tear strength [pli]*
Fibre Glast 2060 Epoxy	418525	1.90	925	-
Smooth-On Mold Star 30	96	339	12500	88
Smooth-On Smooth-Sil 950	272	320	35000	155

3.2 – Fabrication Methods

In order to create composite laminates with integrated hinges, it is necessary to keep the two distinct matrix materials independent from one another. The fabrication techniques used in this study are derived primarily from those developed by White [16] with the intention of being out of autoclave and non-proprietary.

The addition of a secondary matrix system to the composite laminates mandates alterations to conventional composite manufacturing methods. As a means of maintaining the independence of the two matrices, they are infused into the fiber reinforcement and cured individually. The hyper-elastic silicone matrix is impregnated into the hinge regions first, and the stiff epoxy matrix is impregnated into the rest of the laminate second. The presence of the silicone matrix prevents the ingress of the epoxy matrix into the hinge regions, but during the infusion of the silicone, it must be restricted to prevent it from spreading to more area than the desired hinge region. To that end, tape was applied to the carbon fiber fabric to outline the hinge regions and prevent the silicone from spreading outward to areas beyond those desired. Painter's tape was initially used because it sticks to the carbon fiber fabric without bonding and can be removed without warping the woven fabric, but electrical tape later replaced it as the bounding material because it could also be removed easily but created a cleaner silicone boundary. For more intricate origami hinge geometries, the origami was first folded from paper and the folds were highlighted on the paper then copied onto the carbon fiber to provide guide lines for the bounding process. A paper origami fold pattern of a wolf and the corresponding carbon fiber before silicone infusion can be seen in Figure 16. After the boundaries are applied to the carbon fiber fabric, the two-part silicone rubber system is mixed and carefully poured onto the fabric in between the tape boundaries. Light pressure was then applied by hand to ensure impregnation through the thickness of the fabric taking care to keep from spreading the silicone outside of the bounded regions. After the silicone has cured in open air, the excess silicone that cured on top of the bounding material was carefully peeled off to prevent pulling the silicone out of the fiber when removing the bounding material. The

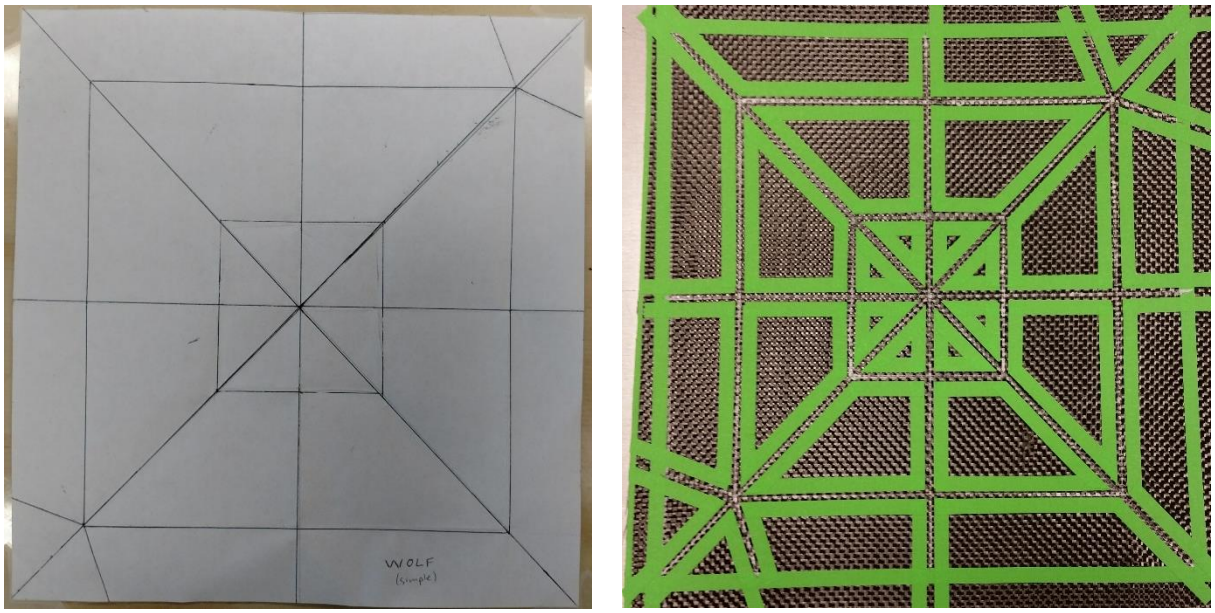

FIGURE 16. PAPER FOLD PATTERN AND PRE-SILICONE-INFUSION BOUNDED CARBON FIBER OF ORIGAMI WOLF

bounding material was then carefully removed in preparation for the epoxy resin infusion. The epoxy resin system was then mixed and applied by hand before vacuum bagging and allowing the epoxy to cure under vacuum. Once the epoxy is cured, the composite is removed from the vacuum bagging setup and any excess material is trimmed away and the composite can be folded.

3.3 – Fabrication Results

Although the tape serves as a boundary for the spread of the silicone, it does not perfectly inhibit the spreading of the silicone. On the top surface where the bounding material is applied, the boundary is usually very clean and sharp. On the underside, however, the silicone often spreads out a bit to the fabric under the bounding material. This phenomenon can be seen in Figure 17. The silicone spread on the underside can be minimized by bounding the hinge regions on both the upper and lower surfaces of the fabric, but for origami fold patterns this is both time consuming and difficult to properly align. During the vacuum bagging process the

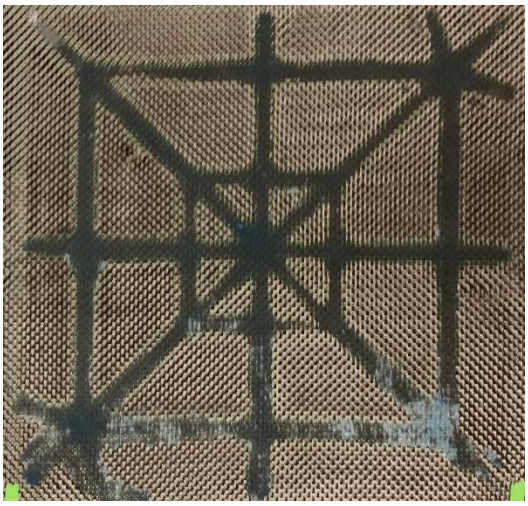

FIGURE 17. SILICONE SPREADING UNDER BOUNDING MATERIAL ON UNDERSIDE OF ORIGAMI WOLF

pressure from the atmosphere often pushes a small amount of epoxy onto the top and bottom of the silicone infused regions; this results in a slightly stiffer first fold and minor cracking can be heard when initially folding.

Several origami structures were fabricated to test the feasibility of the methods described above. A wolf and frog were successfully folded as seen in Figure 18. An origami crane was also fabricated and folded and can be seen in Figure 19. The crane was fabricated using a 1k carbon fiber plain-woven fabric because the thinner fabric is not as severely affected by the stacking and overlapping of multiple layers due to the folding pattern. A Miura sheet was fabricated and its folding stages can be seen in Figure 20.

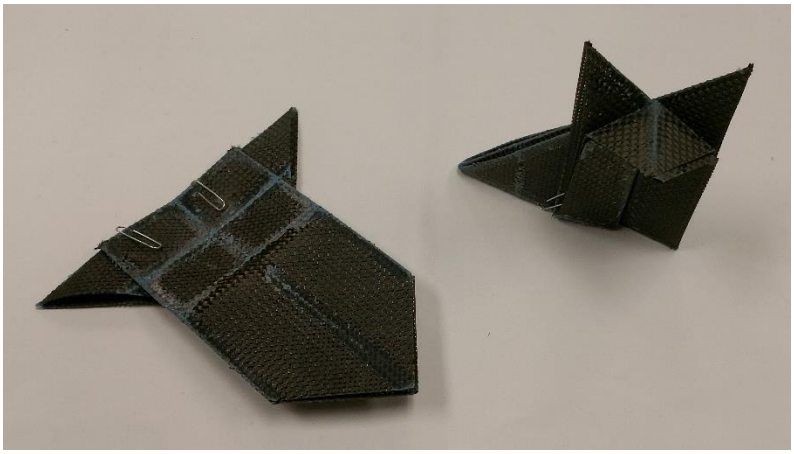

FIGURE 18. CARBON FIBER ORIGAMI FROG AND WOLF

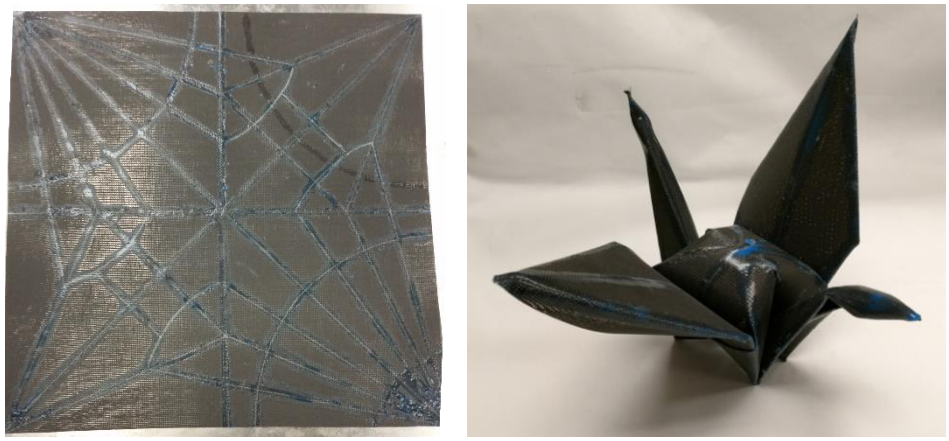

FIGURE 19. UNFOLDED AND FOLDED CARBON FIBER ORIGAMI CRANE

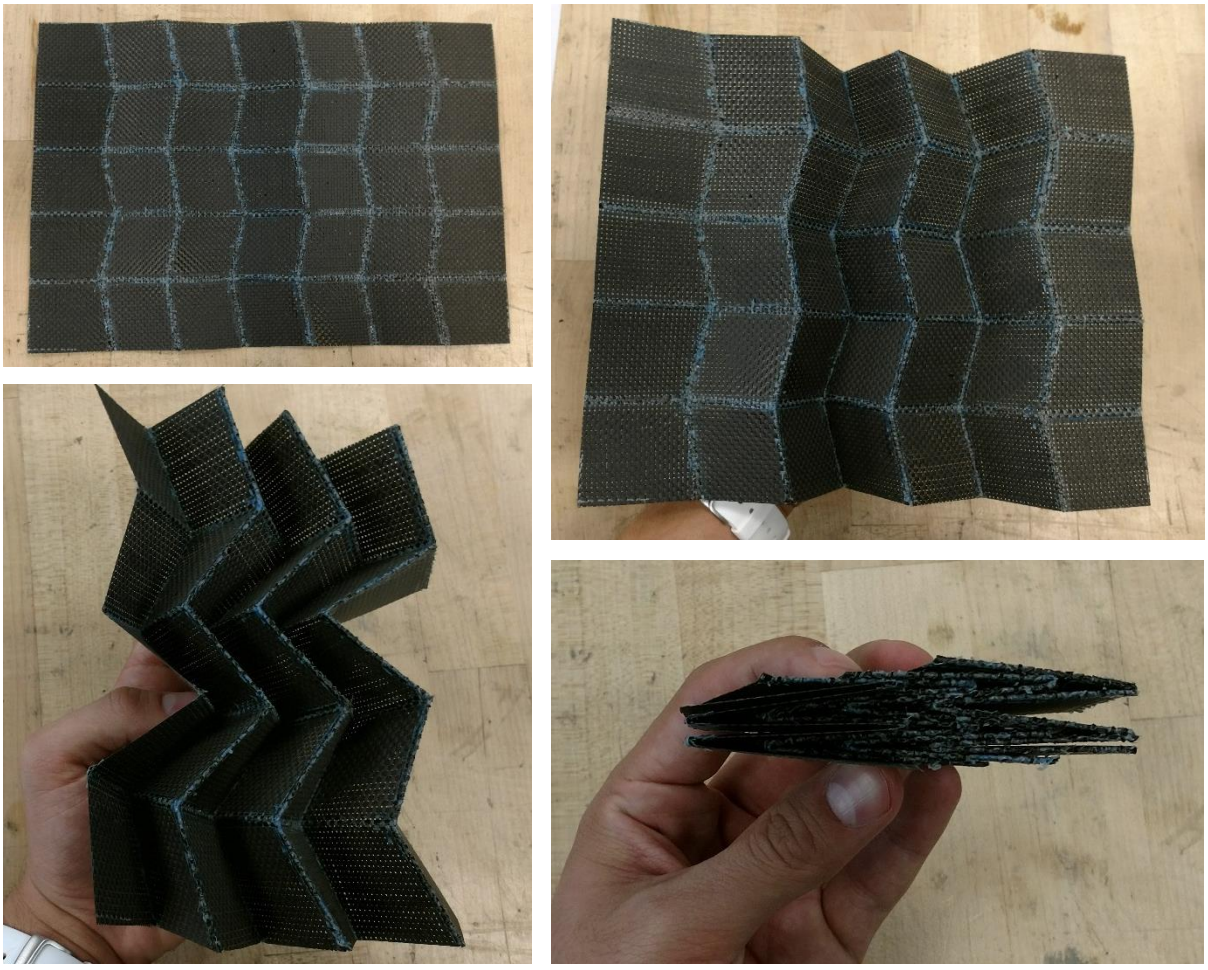

FIGURE 20. FOLDING OF DUAL-MATRIX COMPOSITE MIURA SHEET

A Miura tube was fabricated using dual-matrix composite materials. A small four-cell long tube was made as a representative unit of the tube structure to prove the feasibility. The structure of the tube cannot be made from a single flat piece of material so it was necessary to fabricate the two halves separately and join them subsequently. Each half was fabricated with tabs on either side for joining the halves together. The bounded and fully infused halves can be seen in Figure 21. When assembling the halves it was found that having two sets of tabs on each side caused interference between the sets, so one redundant set of tabs was removed from each half. After cutting the excess material off each half, the two halves were glued together to form the completed tube which can be seen in Figure 22. The tube flattens at no extension

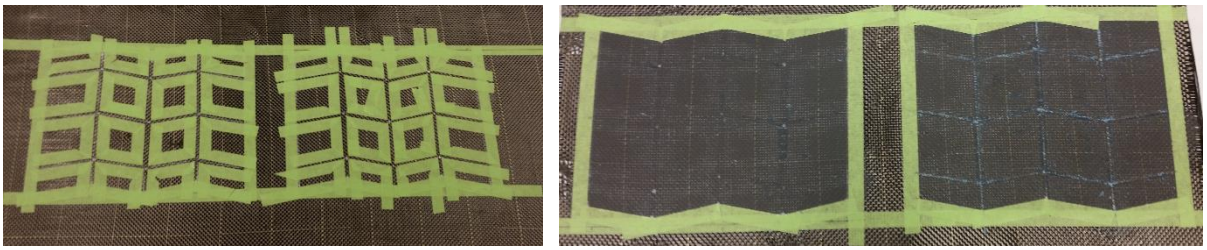

FIGURE 21. BOUNDED AND FULLY INFUSED HALVES OF MIURA TUBE

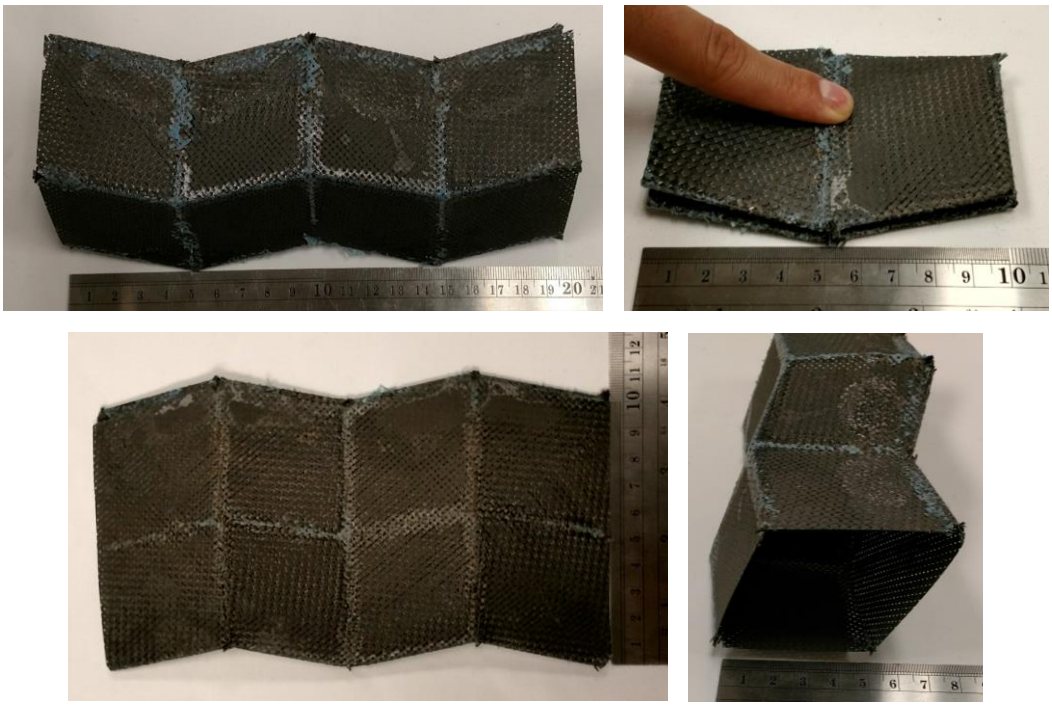

FIGURE 22. VARIOUS CONFIGURATIONS OF COMPLETED DUAL-MATRIX COMPOSITE MIURA TUBE

and full extension like the paper equivalents and shows promise on its own as a self-deploying, packable boom that could be applied to space missions.

3.4 – Comparison of Traditional Origami to Composite Origami

The hinges in the dual-matrix composite origami structures contain significantly more strain energy than their paper equivalents. As a result, the hinges have a high tendency to return to their unfolded state. The difference between the carbon fiber and paper origami is immediately evident when comparing the two origami frogs. As seen in Figure 23, the carbon frog jumps more than four times as high as the paper frog. This high retained strain energy is beneficial

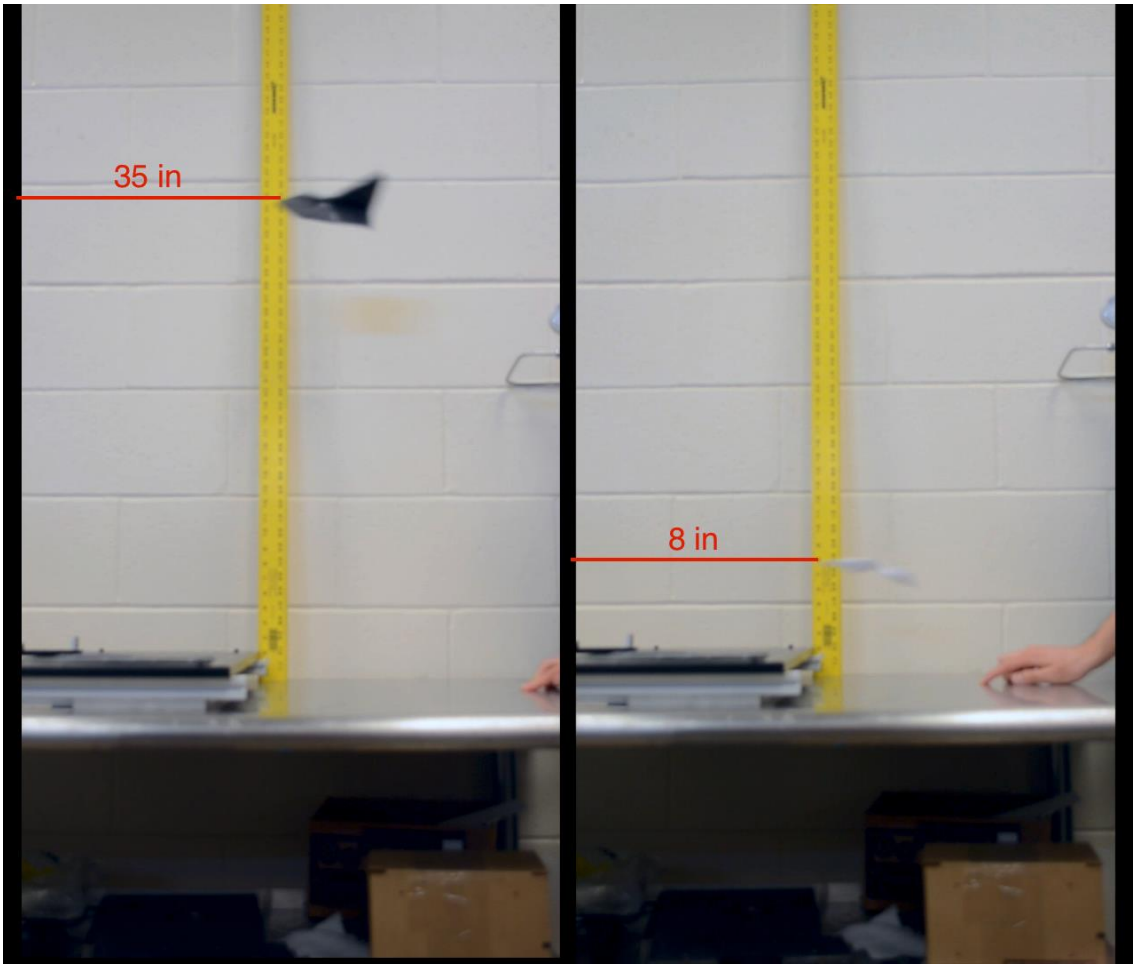

FIGURE 23. COMPARISON OF JUMP HEIGHTS OF CARBON FIBER AND PAPER ORIGAMI FROGS

to deployable structures because it allows for self-deploying structures that rely only on internal strain energy introduced when packaging the structure.

3.5 – Challenges of Hand Fabrication

When it comes to fabricating complex hinge geometries, there are many challenges that present themselves. The nature of origami mandates that the fold locations are highly accurate. When folding paper origami, if the folds are slightly off it can prevent the final structure from folding properly. This effect is amplified by the highly stiff panels of origami dual-matrix composites; if the hinges are slightly misaligned it can result in a structure that will not fold.

The Miura tube as discussed above that was fabricated exhibited the problem of inability to fold. The hinges appeared to be accurate, but they were far enough off to prevent the tube from reaching zero extension and the associated flattening which can be seen in Figure 24. After a few failed efforts a stencil, which can be seen in Figure 25, was laser cut to ensure the guide lines were as accurate as possible when applying the bounding material. With the accurate stenciled guide lines it was possible to fabricate a Miura tube that flattened as intended. Great care had to be taken when gluing the halves together because tabs that are attached only slightly out of the required position can negate near-perfect hinge locations.

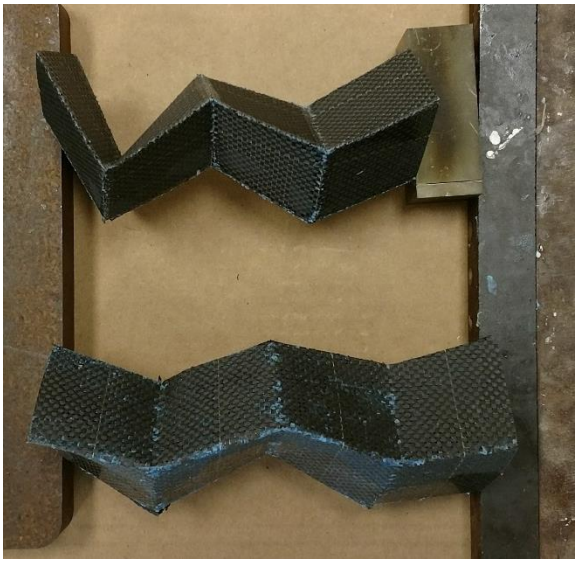

FIGURE 24. MIURA TUBES UNABLE TO FLATTEN DUE TO HINGE MISALIGNMENT

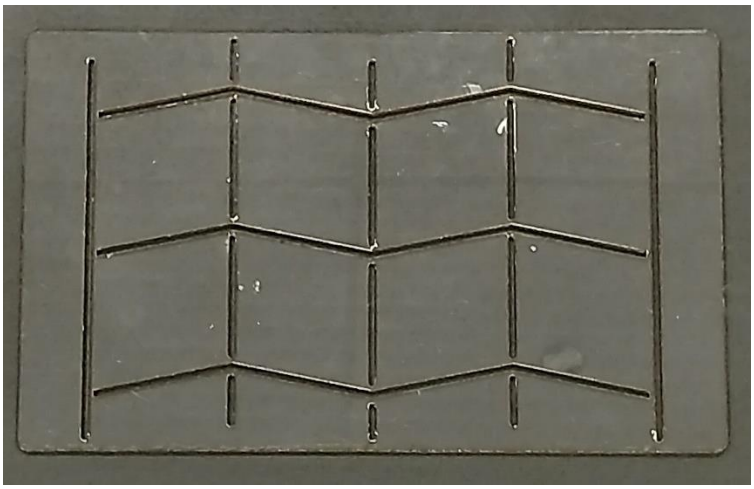

FIGURE 25. LASER CUT MIURA TUBE STENCIL

It is not desirable to have to make a stencil for every dual-matrix composite hinge geometry as it adds an extra step and extra cost to each part. Additionally, even with high-accuracy guide lines, it is still difficult to maintain straight, parallel lines and constant width when applying the tape boundaries for the silicone infusion. Upon close inspection of Figure 26 it can be seen that even for hinges that have only perpendicular intersections the boundaries are not always parallel and the hinges are not of constant width. As such, it is desirable to

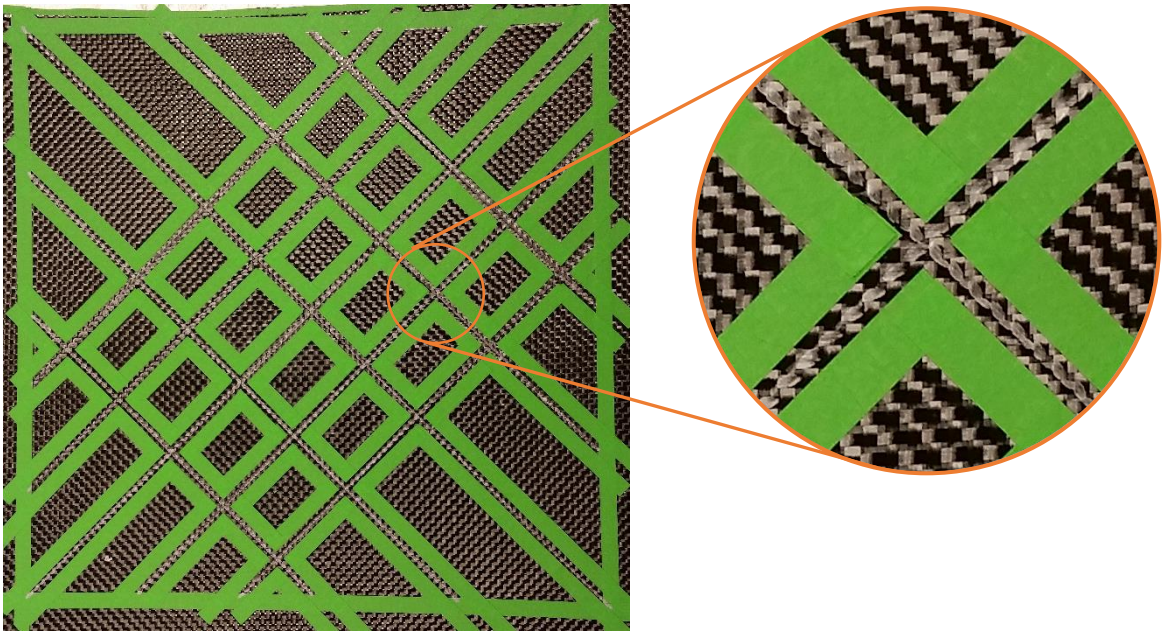

FIGURE 26. INCONSISTENCIES OF HINGE WIDTH AND NONPARALLEL BOUNDARIES OF BOUNDED ORIGAMI FROG PATTERN

develop a method of producing boundaries that are parallel and constant width. To that end, a strip of tape was used as a guide for the application of the bounding tape. Tape was applied atop the silver guide line to serve additionally as a width guide. The hinge will then take on the width of the guide tape as the bounding tape is butted up against the guide tape during application. Once the guide tape and bounding tape are applied, the bounding tape is cut with a razor blade where it overlaps the desired hinge region taking great care not to cut the fibers beneath. A sample composite fabricated using this technique can be seen in Figure 27 with all the tape applied, the guide tape with a red line drawn on it, and with one of the pieces of guide tape and the overlapping bounding tape removed. When the green painter's tape was used it was easy to accidentally cut the fibers with the razor blade, but when using electrical tape this problem was nearly completely mitigated because of the electrical tape's tendency to tear cleanly once cut compared to the painter's tape.

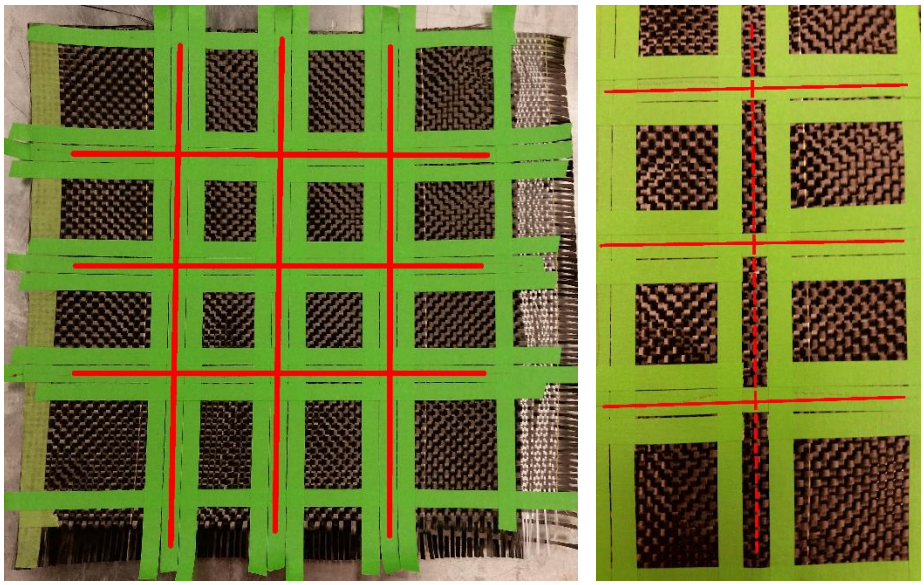

FIGURE 27. SAMPLE COMPOSITE USING GUIDE TAPE (MARKED WITH RED LINE) METHOD AND PARTIALLY REMOVED GUIDE TAPE (DASHED LINE)

Although the electrical tape forms a cleaner silicone boundary than the painter's tape and lessens the fiber damage when removing the guide tape, it is not a perfect solution. Electrical tape is quite stretchy, and while this is nice for fixing damaged wires, it presents a challenge when using it as a bounding material on the carbon fiber fabric. When applying the electrical tape for the hinge area boundaries, great care must be taken to avoid introducing any

elastic strain into the tape by stretching it out. When the tape is released, it will relax to a state of zero or near-zero strain and cause deformation of the carbon fiber fabric it is stuck to. Fabric warping due to tape stretching and relaxation that was experienced during the fabrication of the dual-matrix composite origami crane can be seen in Figure 28. The fabric had to be pulled so that the tape returned to a stretched state and taped down so the fabric would be flat during silicone infusion. Once the silicone was infused and the tape was removed, the epoxy resin was infused without problem.

FIGURE 28. WARPING OF FABRIC DURING CRANE FABRICATION DUE TO TAPE STRETCHING AND RELAXATION

In addition to the logistical challenges of dual-matrix fabrication, there are also environmental considerations that must be made. Like conventional composites fabricated using vacuum bagging techniques, the dual-matrix composite fabrication process generates significant waste that cannot be reused or recycled because of the epoxy resin that impregnates it during fabrication. However, dual-matrix composite fabrication also generates a significant amount of waste in the bounding material. During the bounding process, the tape is cut to very specific shapes determined by the hinge geometry. This results in the bounding material being unusable for other hinge geometries. Even if a second part were desired immediately, it would be exceedingly challenging to replace the bounding material accurately similarly to the challenges discussed earlier in this section on maintaining parallel and consistent width

boundaries. For large, complex parts such as the crane, a lot of bounding material is required to separate the hinge regions from those that will later be infused with epoxy resin. In addition to the bounding tape, the guide tape also goes straight to waste. Often the guide tape has to be torn or cut during removal. All in all, a lot of material goes to waste during dual-matrix composite fabrication.

On the design side of the spectrum, material thickness must be considered if the folded configuration of the structure results in overlapping layers. Given the thickness of the woven carbon fiber fabric, it does not fold as readily as paper. A sample part was fabricated to test how much the layers interfere with one another when complex folds are made. The sample was designed with numerous hinges running the width of the sample and a single long hinge running the length. This allows for the sample to be folded like an accordion along the length then folded in half along the width to observe how easily the stacked layers fold. Using this sample made from a woven 3K carbon fiber fabric, it appears that after two stacking layers it becomes difficult to fold the composite completely flat. The unfolded test part and double-stacked and triple-stacked layer folds can be seen in Figure 29. In order to account for the

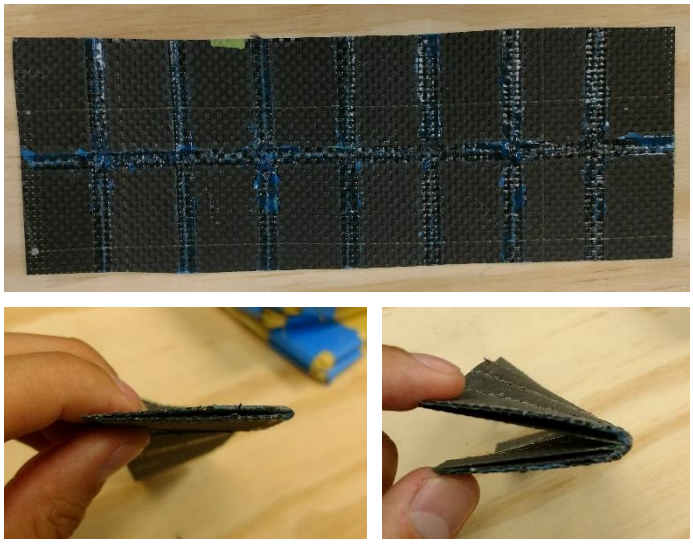

FIGURE 29. THICKNESS INTERFERENCE TESTING SAMPLE: TWO LAYER FLAT FOLD AND INTERFERENCE EXPERIENCED AT THREE LAYERS

thickness of the composite, the hinges that would be on the outside of the fold would have to be wider to allow the hinge to bend around the inner layers. This is completely dependent on

the geometry of the structure and depending on the interactions between the layers it may be unnecessary, but this is the reason the crane was made with 1K fabric over 3K fabric.

3.6 – Inspirations for Plotter

Although the dual-matrix composite fabrication methods detailed above are desirable for their ease of access, they are not the most reliable when fabricating complex origami hinge geometries. As such, it would be beneficial to devise a method of fabrication that offers more consistency and reliability. An optimal fabrication method would ideally eliminate or mitigate all or most of the challenges discussed in the previous section. A novel computer numerical controlled (CNC) silicone infusion system was explored as a means to accurately and consistently infuse the silicone hinges without the need for stencils or more advanced bounding methods. An added benefit of giving the computer the ability to accurately infuse specific regions is the lack of need for bounding material. As a result, it also eliminates all the waste generated by the bounding process. Creation of a CNC plotter for silicone infusion in dual-matrix composite manufacture has the potential to eliminate the boundary inconsistencies and minimize accuracy issues presented and dramatically decrease the waste generated by the previously used fabrication techniques.

Chapter 4 – CNC Plotter for Dual-Matrix Composite Fabrication

A computer numerical control (CNC) plotter inspired by 3D printers was created for reliable and consistent infusion of silicone hinge regions of dual-matrix composites. Mechanization of the silicone infusion process allows for origami hinge geometries to be infused accurately without need for the time consuming and resource intensive bounding process. Computer models of hinge architectures allow for repeated infusions of the same geometry as well as simple modifications.

4.1 – Construction of Plotter

The design of the silicone plotter was inspired by that of a Cartesian fused deposition modeling (FDM) 3D printer on a larger scale. Conventional FDM 3D printers fabricate parts by melting and extruding a polymer filament into specific, predetermined locations to form a solid object. This concept was adapted to selectively infuse a liquid silicone rubber into specific, predetermined regions of a carbon fiber fabric to create complex origami hinge geometries in two dimensions instead of three.

The silicone plotter was designed and constructed using readily available components so it can be reproduced easily. The completed plotter is seen in Figure 30. The frame of the plotter was constructed using 1 inch 8020 extruded t-slotted aluminum to create a modular design to support future expansions and modifications if necessary. Roller carriages were used carry the crossbar that supports the extruder and the extruder assembly that rides along the crossbar. The wheelbase of the crossbar on the *x*-axis was widened to provide stability for the motor that controls the *y*-axis motion that is mounted nearby, see Figure 31. The movement is provided by stepper motors connected to timing belts; the mounts to connect the motors to the frame as well as to hold the timing belt pulley axles were 3D printed, see Figure 32. Unlike the stationary *x*-axis pulley mounts, the *y*-axis pulley mount had to mount onto the crossbar as the entire *y*-axis drivetrain must move with the crossbar. The crossbar is moved along the *x*-axis by a stepper motor connected to a driveshaft that drives both ends of the crossbar simultaneously to prevent the roller carriage wheels from jamming due to the length of the *y*-

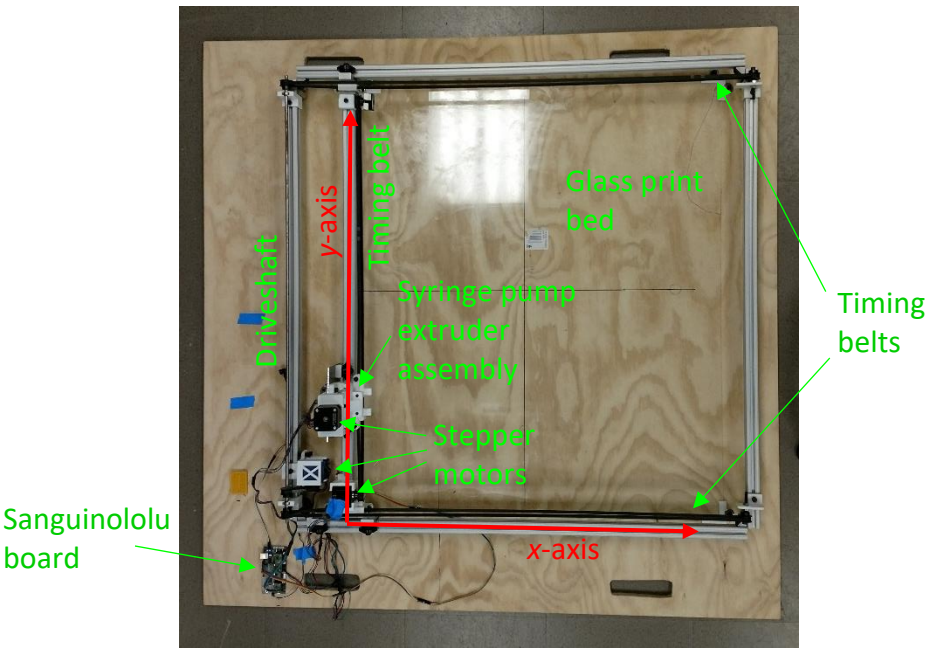

FIGURE 30. SILICONE PLOTTER

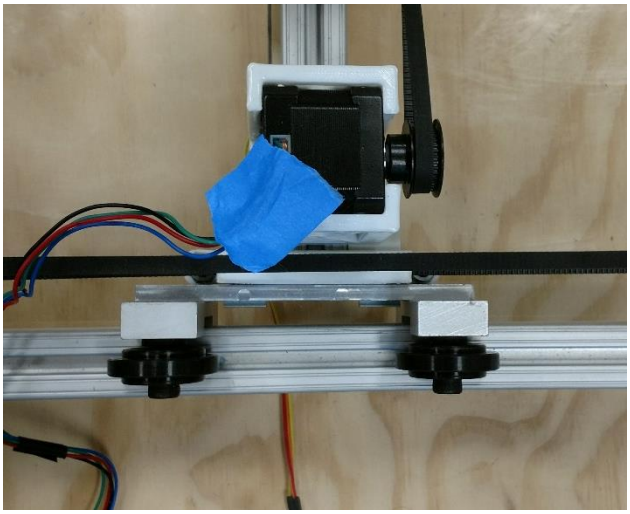

FIGURE 31. WIDENED WHEELBASE FOR *Y*-AXIS STABILITY

axis crossbar. The bearing mounts for the driveshaft were also 3D printed, one can be seen in the left image of Figure 32. The extruder assembly is a 3D printed, open source syringe pump mounted to a plate connecting two roller carriages. Mechanical end stops serve as the zero limit on both axes. The *y*-axis end stop and its 3D printed mount can be seen in Figure 33. The plotter frame was bolted to plywood to facilitate transport and prevent misaligning the

FIGURE 32. 3D PRINTED MOTOR MOUNT AND TIMING BELT PULLEY AXLE MOUNTS

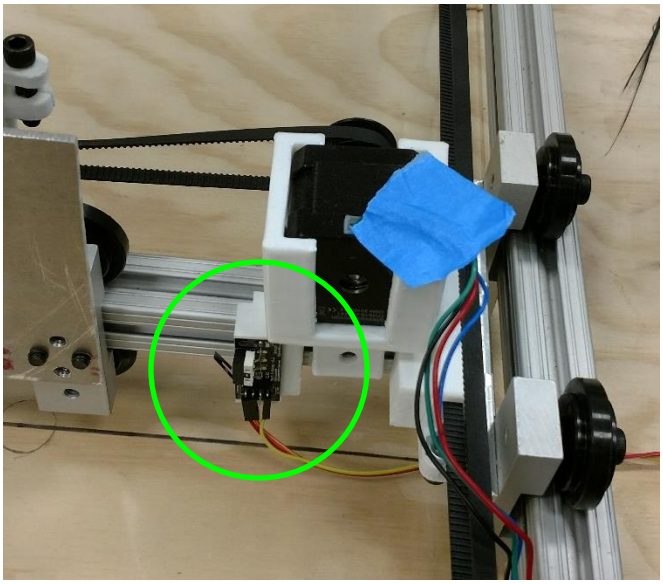

FIGURE 33. *Y*-AXIS END STOP AND 3D PRINTED MOUNT

FIGURE 34. GLASS PRINT BED AND ATTACHMENT BRACKET

frame, and a glass pane was attached with brackets to provide a flat, nonporous print bed surface, see Figure 34. The stepper motors' movements are controlled by a Sanguinololu

1.3B2 board and Pololulu A4988 stepper motor drivers. Power is provided to the plotter by a 1 A, 12 V power supply. A resistor was connected to the thermistor pins on the board to provide a constant temperature and satisfy an extruder temperature signal requirement. Figure 35 shows the configuration of the Sanguinololu board.

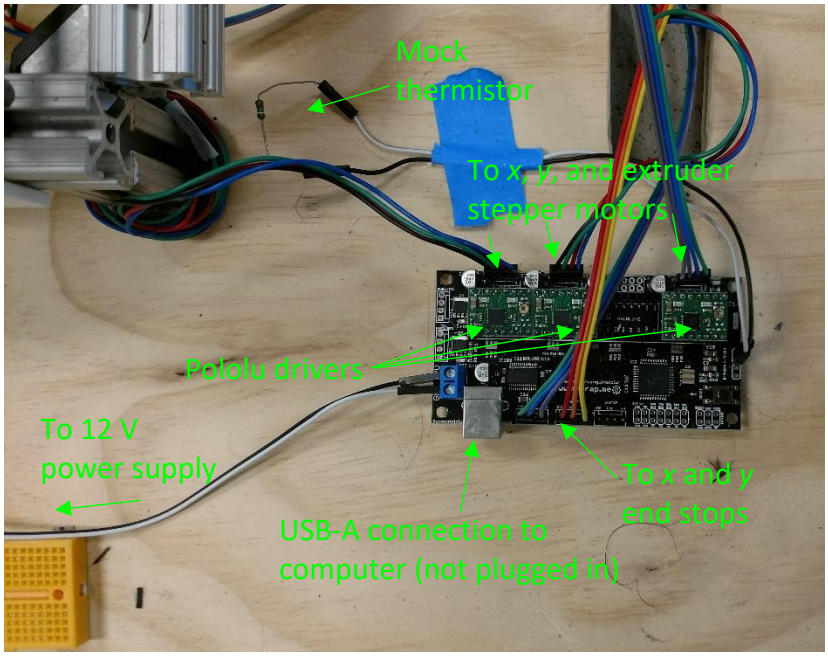

FIGURE 35. SANGUINOLOLU BOARD CONFIGURATION

The hardware specifications of the silicone plotter can be seen in . The silicone plotter has a print area of 640 mm × 600 mm. This allows for silicone infusion of large carbon fiber fabric specimens. A cross was marked on the plywood under the glass bed to assist in centering the fabric on the bed; the software automatically centers the model on the print bed. Before running the plotter, mold release is applied to the glass bed so that the silicone will not stick to the glass during curing. Once the glass bed surface is prepared, a slightly oversized piece of carbon fiber fabric is taped to the bed using a 1.5-inch-wide painter's tape as can be seen in Figure 36. The painter's tape serves as a ramp to prevent the extruder from catching on the edge of the fabric which could move the fabric or misalign the extruder, and the carbon is intentionally oversized so the extruder will not have to cross the tape threshold more than once per print. A polytetrafluoroethylene (PTFE) O-ring was connected to the bottom of the syringe with a 3D printed adapter as seen in Figure 37. This both provided a source of pressure to

infuse the silicone into the carbon fiber fabric and served as a stabilization mechanism for the top-heavy extruder assembly.

FIGURE 36. CARBON FIBER SAMPLE BEFORE SILICONE INFUSION USING PLOTTER

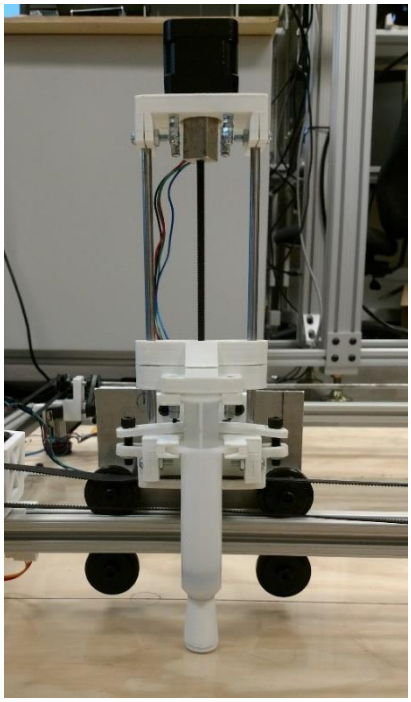

FIGURE 37. SYRINGE PUMP EXTRUDER ASSEMBLY

TABLE 2. HARDWARE SPECIFICATIONS OF PLOTTER

Print Area	640 mm × 600 mm
Resolution	23 µm
Nozzle Width	1.25 mm
Print Surface	Glass
Compatible Materials	Liquid resin systems
Firmware	RepRap Sprinter
Communications	USB

4.2 – Controlling the Plotter

In keeping with the accessibility of the plotter, all the software used to run the plotter is open-source. The motherboard that controls the plotter is a Sanguinololu 1.3B2 board specifically designed for use in 3D printers. Sanguinololu was chosen because it is an all-in-one solution for the electronics and did not require electrical work beyond soldering the pins and connectors onto the board. When combined with Pololu compatible stepper motor driver boards the Sanguinololu can easily control the four axes of a 3D printer: *x*, *y*, *z*, and the extruder. For the silicone plotter the *z* axis is ignored since it only infuses silicone into a flat carbon fiber fabric.

RepRap is a popular 3D printing solution known for its self-replicating capabilities. The RepRap project is also a valuable source of information regarding 3D printing. The firmware that controls the silicone plotter is Sprinter from the RepRap project. Sprinter was chosen because it is simple but robust allowing for ease of use but also the freedom to make the necessary modifications to adapt a 3D printing firmware to a large 2D silicone plotter. Sprinter was configured to the specifications of the motherboard, stepper motors, and timing belt hardware used in the silicone plotter project so the information received and signals sent by the computer correspond to accurate real world movements. The configuration parameters of the silicone plotter can easily be altered using the Arduino software and are found in Appendix A.

Like 3D printers, the plotter uses G-code to control its movements. The firmware onboard the Sanguinololu microcontroller interprets the G-code, but in order for the plotter to be able to interface with the computer, it is necessary to have a host software program to send

the G-code to the plotter's microcontroller to be executed. For the silicone plotter, Pronterface was chosen as the host software because it is simple to use and provides an intuitive, customizable graphical user interface. To generate the G-code to send to the printer it is necessary to have a slicing software. Here, Slic3r was chosen for its ease of use. The Slic3r configuration parameters were adjusted to match the silicone plotter hardware and can be found in Appendix BAppendix B – Slic3r Configuration Bundle for Silicone Plotter. It is crucial to have the same settings for the print area in both the host and slicing software otherwise the full area of the bed will not be used. Like Sprinter, Pronterface and Slic3r are both open-source software.

With the software infrastructure in place, infusing the silicone into the carbon fiber fabric is very straightforward. Similarly to the hand fabrication methods, a pattern of the hinge geometry must be created. Using any 3D CAD modeling software—SolidWorks was used in this research—a three-dimensional model of the hinge geometry can be created and saved as an .STL file, the same filetype as those used in 3D printing. By setting the model thickness to that of a single layer as interpreted by the slicing software, in this case 0.3 mm, the plotter will make a single infusion pass over the specified regions. Increasing the model thickness will result in multiple infusion passes over the hinge regions. Once the .STL file of the hinge geometry is created, it can be imported into the slicing software to be sliced then loaded into the host software to be sent to the silicone plotter and plotted. The Slic3r and Pronterface

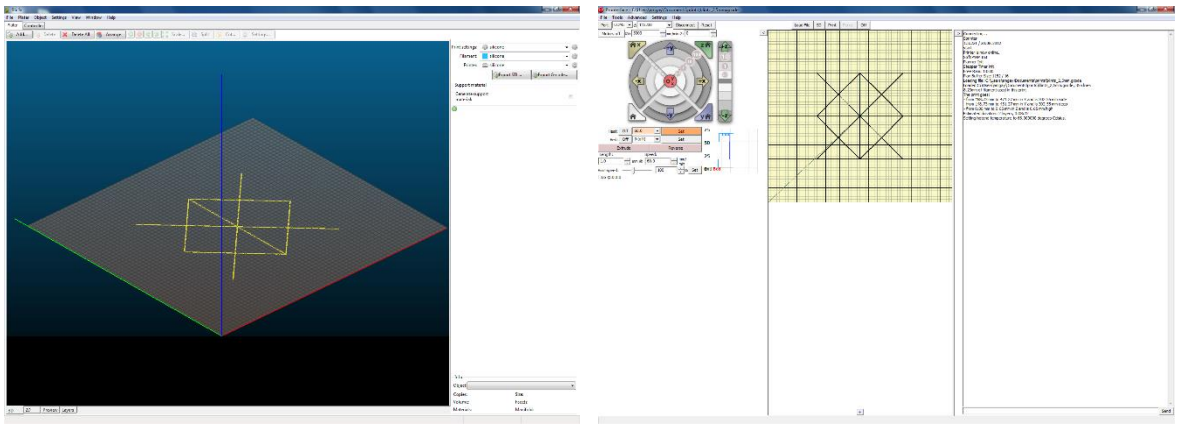

FIGURE 38. SLIC3R AND PRONTERFACE VIEWS OF BLINTZ ORIGAMI HINGE GEOMETRY TO BE PLOTTED

views of a Blintz origami hinge geometry to be plotted can be seen in Figure 38. The G-code for the blintz model sliced and run in this test can be found in Appendix C.

4.3 – CNC Plotter Results

With the hardware and software of the silicone plotter operating smoothly, testing its dual-matrix fabrication capabilities can begin. Initial tests were simple straight-line hinges to test the infusion of the silicone through the fabric. As seen in Figure 39, the silicone beaded up on top of the carbon fiber fabric and did not flow into it at all. It was also observed that degassing the silicone using a vacuum chamber after mixing and before filling the syringe produced much

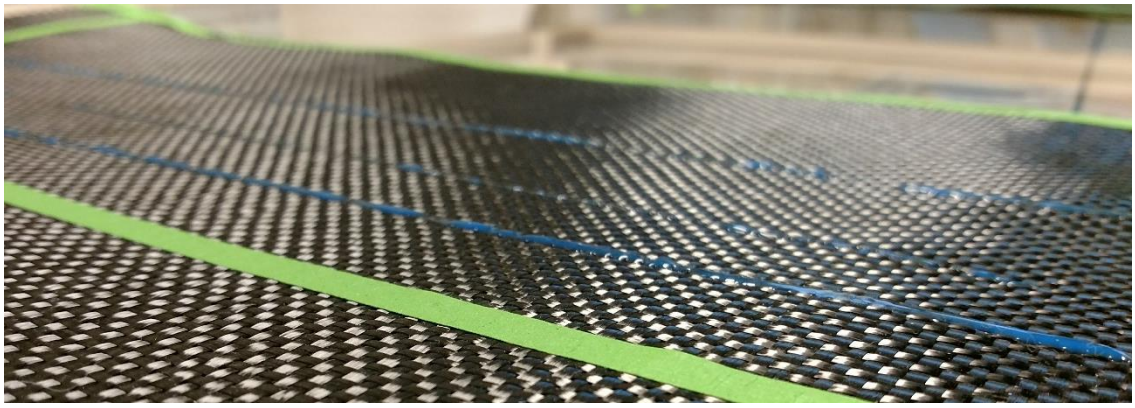

FIGURE 39. SILICONE THAT FAILED TO IMPREGNATE FABRIC (PRE-PTFE O-RING)

more consistent silicone output. The lack of through-thickness impregnation led to the incorporation of the PTFE O-ring discussed previously. The O-ring applies pressure to the silicone after it is laid down on the fabric by the syringe and impregnates it through the fabric. With the O-ring providing adequate impregnation through the fabric, the amount of silicone infused was altered to see how the changes would be reflected in the hinge regions. Hinges of three different widths and three different thicknesses were modeled for a total of nine test hinge templates, which can be seen in Table 3, to determine the parameters to use going forward. The results of the width and thickness test can be seen in Figure 40. The silicone of the leftmost test hinge was very sparse due to a small air pocket in the bottom of the syringe at the start of the test. After this test, a small amount of silicone was extruded at the beginning of each test to minimize the air present in the syringe. The hinge lines have an unintended diagonal line

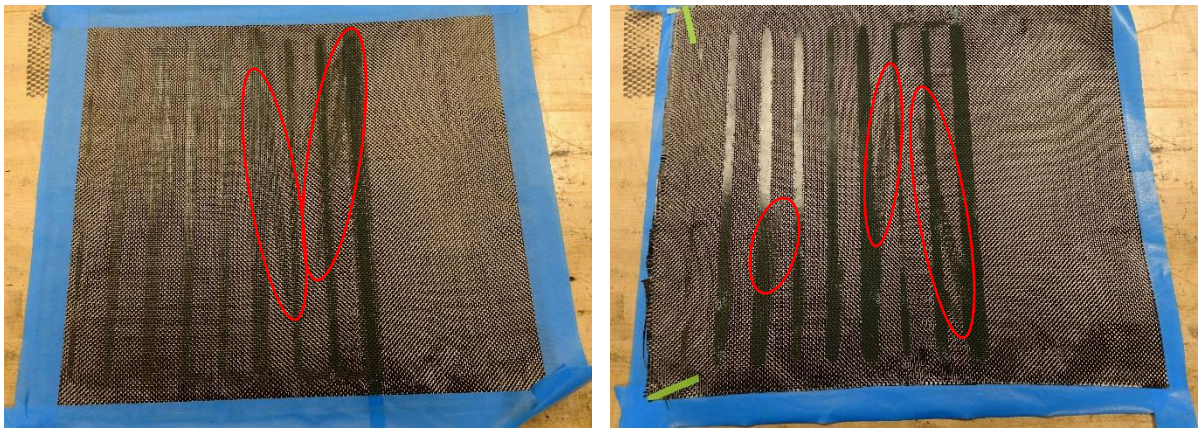

FIGURE 40. TOP AND UNDERSIDE OF WIDTH AND THICKNESS TESTS (INCREASING WIDTH AND THICKNESS FROM LEFT TO RIGHT), 'BARBS' HIGHLIGHTED

similar in appearance to a barb that resulted from excess silicone buildup inside the O-ring adapter that was dragged toward the start point of the next hinge line. The two- and three-infusion passes (0.6 mm and 0.9 mm model thickness, respectively) hinges showed much more consistency within the hinge than the single layer. However, the three-infusion pass yielded much more material and spread it out to a much wider area than intended. Because of these two factors, the two-infusion pass method was the one chosen to explore moving forward. After further testing, a hinge width of 1.5 mm was chosen because it didn't spread as extensively as a 2 mm hinge and a 1 mm hinge experienced difficulty in the slicing software when combined with multiple layers. With the hinge geometry determined, three simple hinge samples were fabricated to compare the hand fabricated hinge to the plotted hinge and two plotted hinges using different silicone systems, see Figure 41.

TABLE 3. TEST HINGE MODEL PARAMETERS

Hinge Thickness	*Corresponding Infusion Passes*	*Hinge Width*
0.3 mm	1	2 mm
		3 mm
		4 mm
0.6 mm	2	2 mm
		3 mm
		4 mm
0.9 mm	3	2 mm
		3 mm
		4 mm

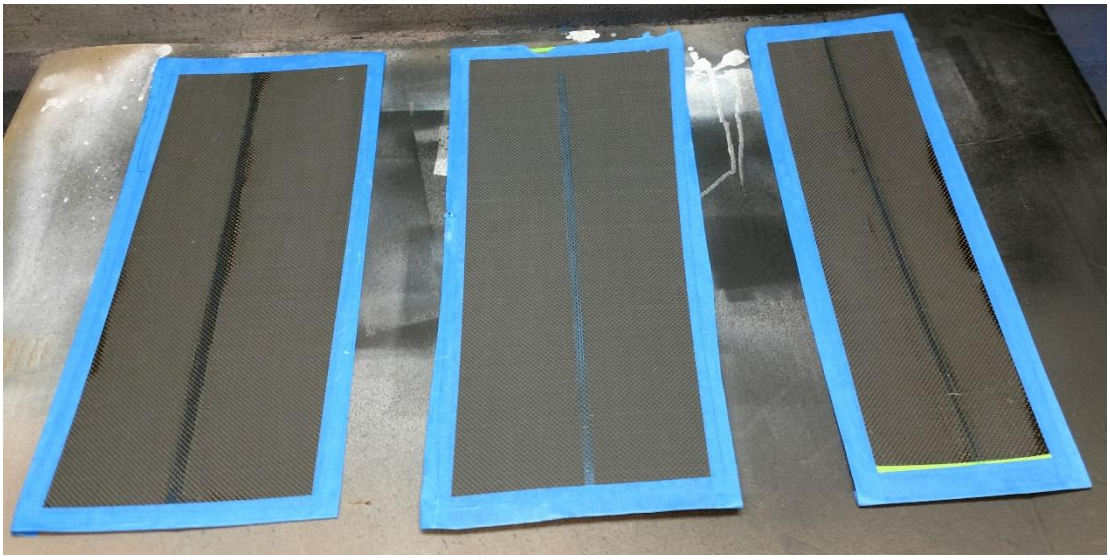

FIGURE 41. SIMPLE HINGE SPECIMENS FOR TESTING

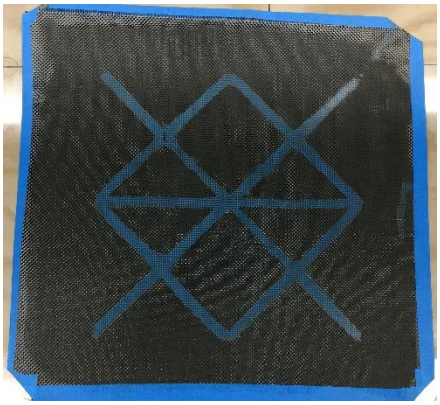

FIGURE 42. BLINTZ ORIGAMI FOLD PATTERN

To demonstrate the plotter's ability to easily fabricate more complex origami hinge geometries, a blintz origami pattern was made using dual-matrix composites. The hinge geometry can be seen in Figure 42, and the folding process can be seen in Figure 43. The blintz pattern further demonstrates that it is possible to implement dual-matrix composites into small-packing applications. The original blintz pattern was made with a 1.5 mm hinge, but it didn't fold perfectly flat in the final state, so it was remade using a 2.5 mm hinge. The plotter took just over eight minutes to infuse the blintz geometry into the fabric, a process that would likely take upwards of an hour if bounding by hand like discussed in the previous chapter. The

2.5 mm hinge blintz pattern folded more easily than the 1.5 mm hinge version, but it exhibited fiber breakage within the hinges as seen in Figure 44 which implies that the epoxy resin was able to permeate the hinge region where silicone should have been. It is suspected that the O-ring infuser may be applying too much pressure and forcing the silicone out of the hinge regions.

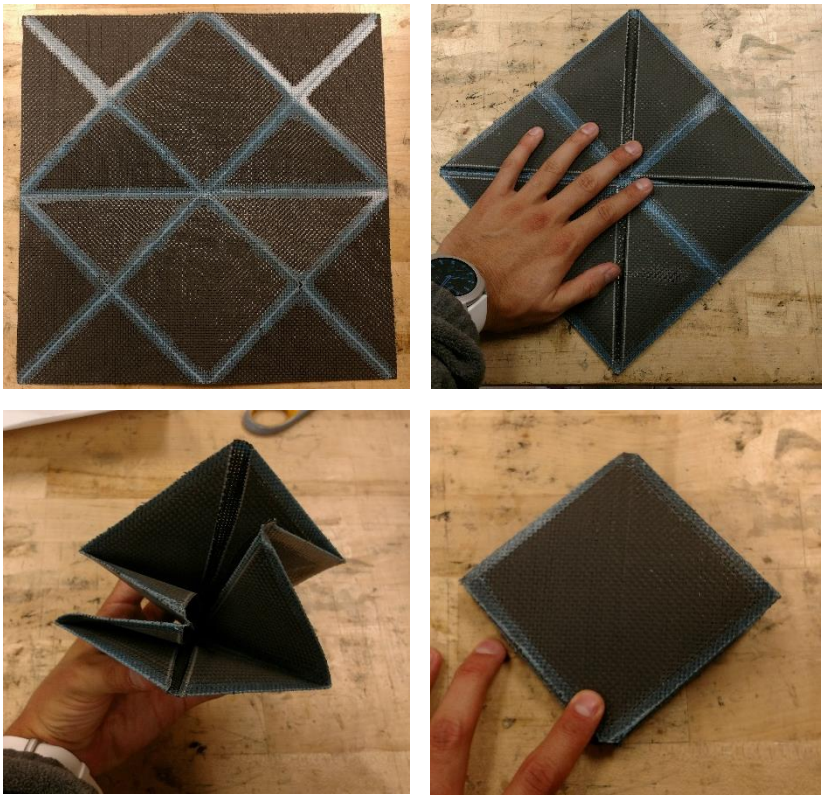

FIGURE 43. BLINTZ ORIGAMI FOLDING PROCESS

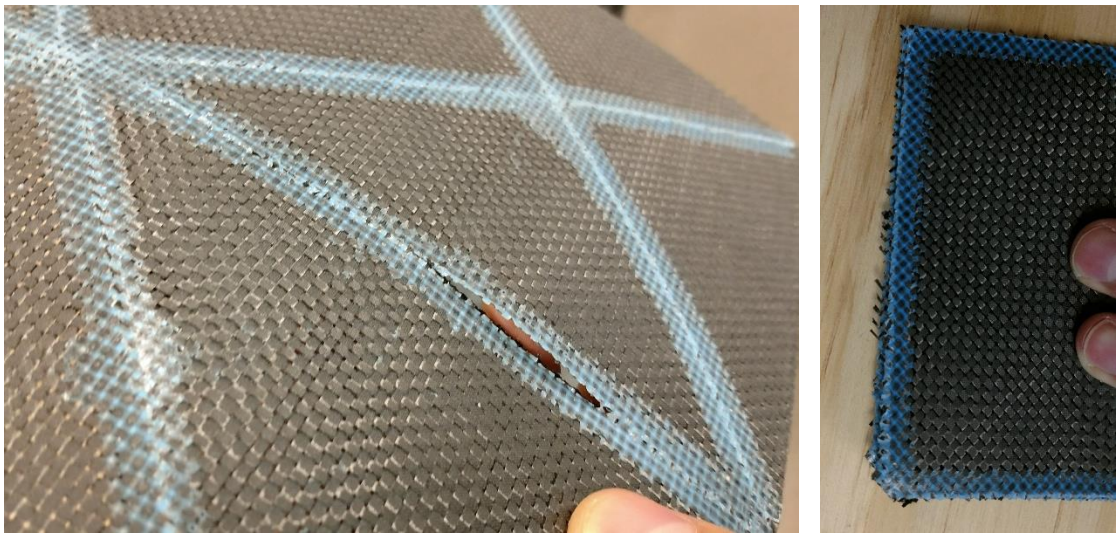

FIGURE 44. FIBER BREAKAGES WITHIN HINGES OF BLINTZ ORIGAMI

4.4 – Conclusions

A plotter was designed and constructed to infuse silicone hinges into carbon fiber for origami architectures in dual-matrix composites. The plotter exhibits higher accuracy and repeatability of hinge geometry than prior hand fabrication methods. Complex hinge geometries were infused in a fraction of the time hand fabrication would allow. Further optimization is necessary to ensure thorough impregnation of the fabric and eliminate excess silicone outside hinge regions. With the plotter producing consistent composite parts, it is important to determine the material properties of those parts to understand how they will behave before they can be implemented into flight-worthy applications.

Chapter 5 – Mechanical Characterization of Dual-Matrix Composites

Mechanical characterization tests of dual-matrix composite coupons are developed to impart near pure bending deformation. Loading in compression was applied using an Instron 8502 load frame equipped with a fixture designed to isolate bending and provide a large range of motion of the bend. Three-dimensional digital image correlation (3D DIC) software was used to capture the deformation of the sample during testing.

5.1 – Testing Setup

Testing was done using an Instron 8502 load frame and a 10 N load cell. Each sample was loaded into a novel fixture designed to induce near pure bending. The fixture was developed in concurrent work and applies a moment to the initially flat sample through an offset compressive load, see Figure 45 and Figure 46 [22]. The test cycled each sample from nearly flat to a 90° bend angle and back, twice. The test was started with the sample slightly pre-buckled to prevent it from bending away from the cameras and into the fixture. The test was

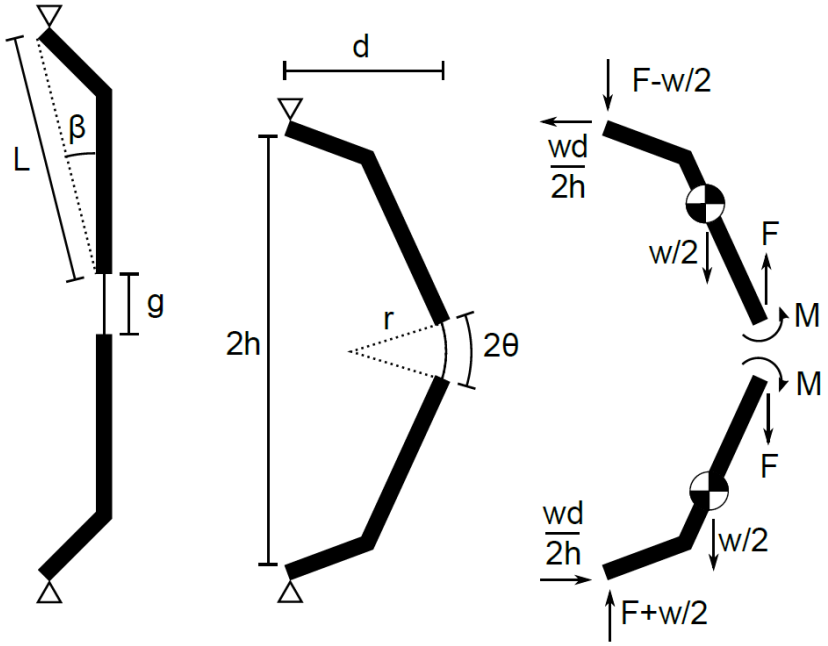

FIGURE 45. SCHEMATIC OF BENDING FIXTURE [22]

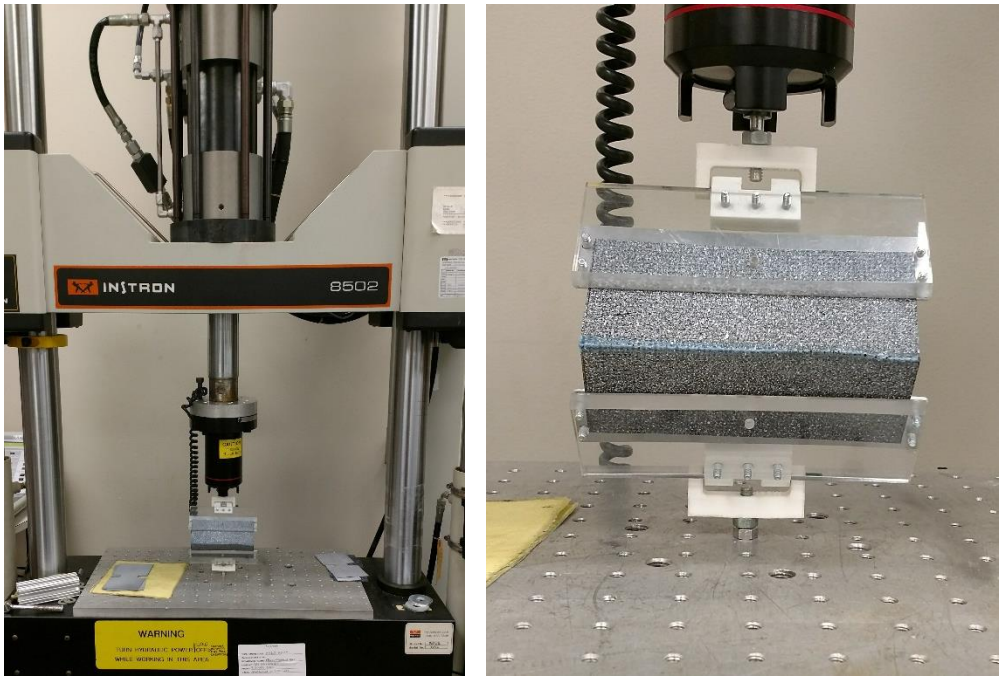

FIGURE 46. BENDING TEST SETUP IN INSTRON LOAD FRAME AND CLOSEUP OF TEST SPECIMEN

stopped at 90° because past that point the weight of the fixture starts to influence the bending and force measurements. The undeformed gauge length of the mounted sample was 50 mm for each coupon. During the testing, the Instron load frame recorded the force information, and knowing the force required to bend the sample and the geometry of the fixture allows for calculation of the bending moment. Unlike single-matrix thin laminates, the curvature cannot be accurately calculated using test parameters, so it must be obtained by other means. In this research, 3D DIC was used to capture the deformation of the sample. The DIC setup consisted of two 5 megapixel Point Grey Grasshopper2 cameras equipped with 67 mm lenses. The DIC setup captured the deformation of the composite sample at one second intervals throughout the test; the images captured were used to calculate the curvature using Vic-3D 7, see Figure 47.

Three dual-matrix composite samples previously fabricated were tested to determine the bending stiffness of the materials. Two samples were fabricated using the Mold Star 30 silicone, one sample by hand and one with the plotter, to determine the difference, if any, between the two manufacturing methods. The third sample was fabricated using the Smooth-Sil 950 silicone and the plotter to compare the two silicone matrix systems. All three samples

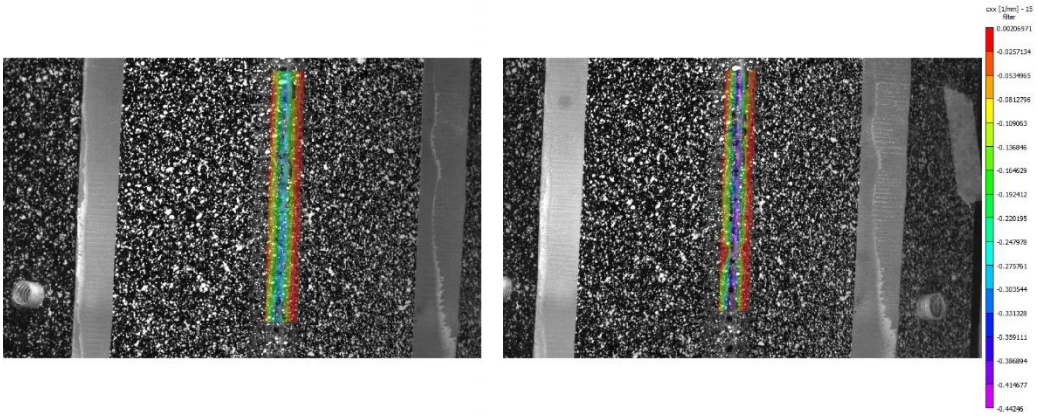

FIGURE 47. VIC-3D OVERLAY OF CALCULATED CURVATURE AT TWO POINTS DURING BENDING TEST

were fabricated with the weave of the fabric in the 0-90° direction. The samples were speckled using white spray paint by spraying paint over each sample and allowing paint droplets to fall onto the surface of the sample. The speckle pattern allows the 3D DIC software to capture information about the deformation of the sample. A base coat of paint was not applied because it cracks and flakes off when the sample is subjected to the extreme bending. Each sample was then cut into three coupons five inches wide. The coupons were individually mounted into the fixture and loaded into the load frame, see Figure 46. Each coupon was bent prior to testing to eliminate the effect of a stiffer first bend due to epoxy resin that wicks on top of and underneath the silicone hinges during the vacuum bagging.

5.2 – Material Properties

Once the force data had been obtained from the test, the bending moment can be calculated using the geometry of the fixture and sample and the following equations.

$$h = \frac{g}{2\theta} sin\,\theta + L\cos(\theta + \beta)$$

$$d = \frac{g}{2\theta}(1 - \cos\theta) + L\sin(\theta + \beta)$$

$$M = \left(F - \frac{w}{4}\right) d$$

By plotting the moment versus curvature and assigning a trendline, the bending stiffness of the sample can be found in the slope of the line. The bending stiffness of each of the three test

coupons was found then three values were averaged to find a representative value for the bending stiffness of each sample, see Table 4. Unlike the hand fabricated and plotted Mold Star 30 samples (HMS30-1 and PMS30-1, respectively) the plotted Smooth-Sil 950 sample (PSS950-1) only had two bending stiffness values to average. The sample was not pre-bent before the speckle pattern was applied, so some of the speckle pattern was disrupted when the epoxy cracked off the silicone. Because of this, the DIC system had difficulty tracking the speckles and thus was unable to calculate the curvature of the hinge. The graphs of moment versus curvature for each sample can be seen in FIGS. The values are negative because of moment conventions and how the DIC software defines curvature. All the samples returned to a completely un-bent state after being removed from the test fixture.

TABLE 4. BENDING STIFFNESS OF DUAL-MATRIX COMPOSITE COUPONS

Sample	*Bending Stiffness [N mm²]*			
	Test 1	*Test 2*	*Test 3*	*Sample Average*
HMS30-1	0.9382	0.8299	0.9496	0.9059
PMS30-1	0.7972	1.8123	0.8591	1.1562
PSS950-1	1.0758	1.2386	-	1.1572

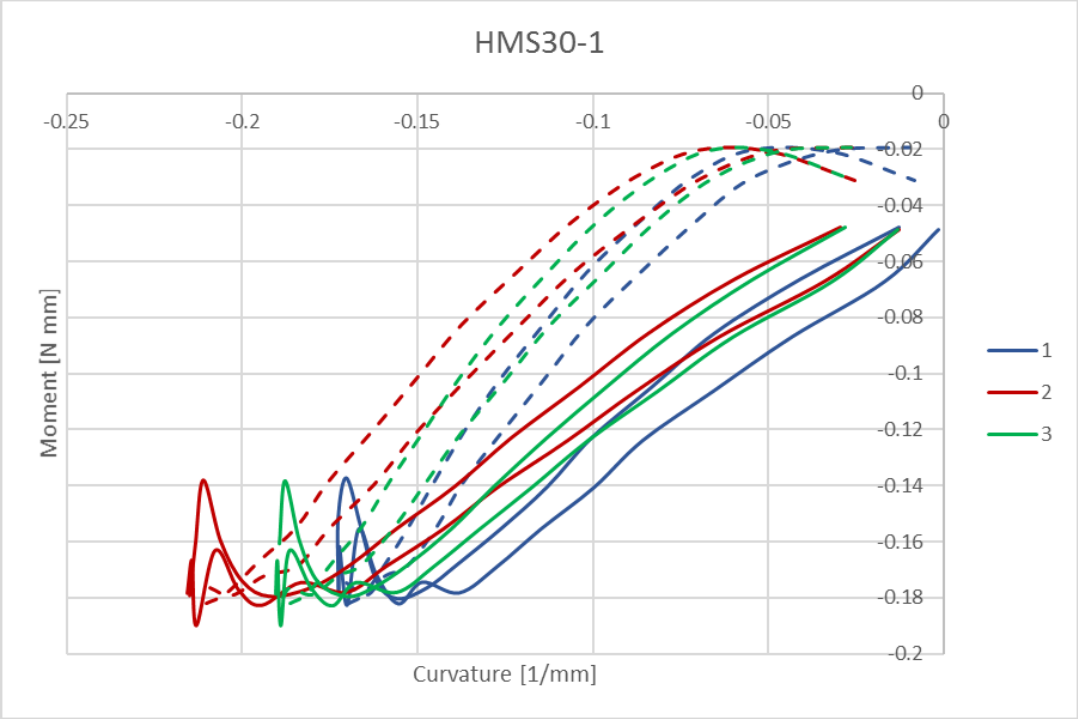

FIGURE 48. MOMENT VS. CURVATURE OF HAND FABRICATED MOLD STAR 30 SAMPLE (SOLID LOADING, DASHED UNLOADING)

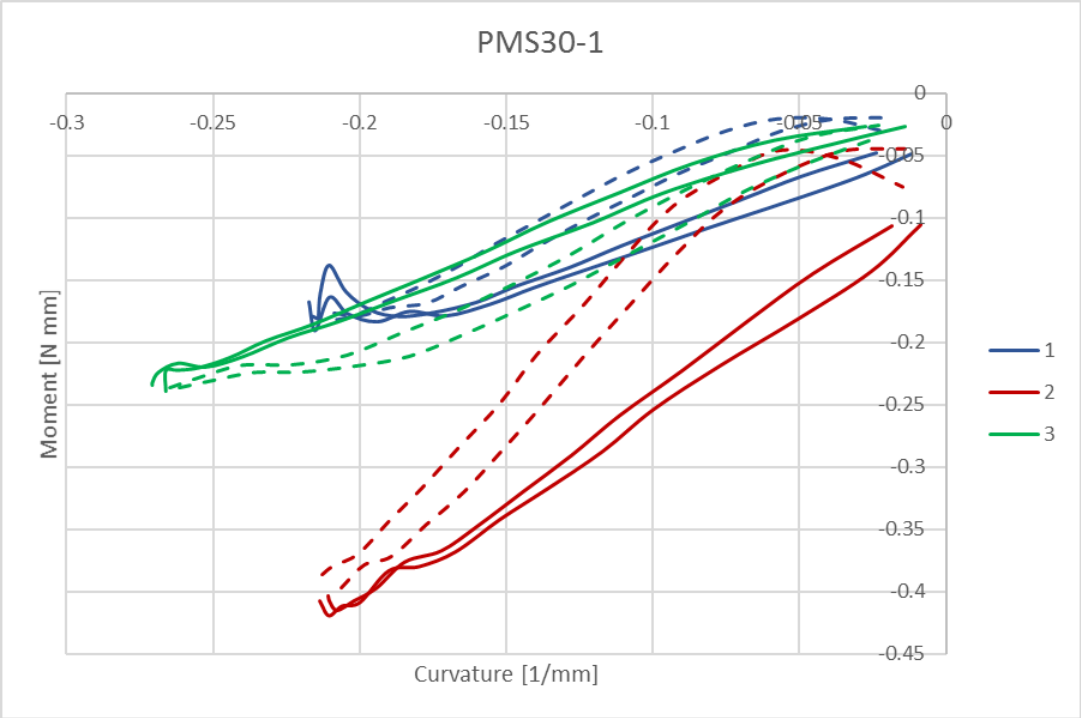

FIGURE 49. MOMENT VS. CURVATURE OF PLOTTED MOLD STAR 30 SAMPLE (SOLID LOADING, DASHED UNLOADING)

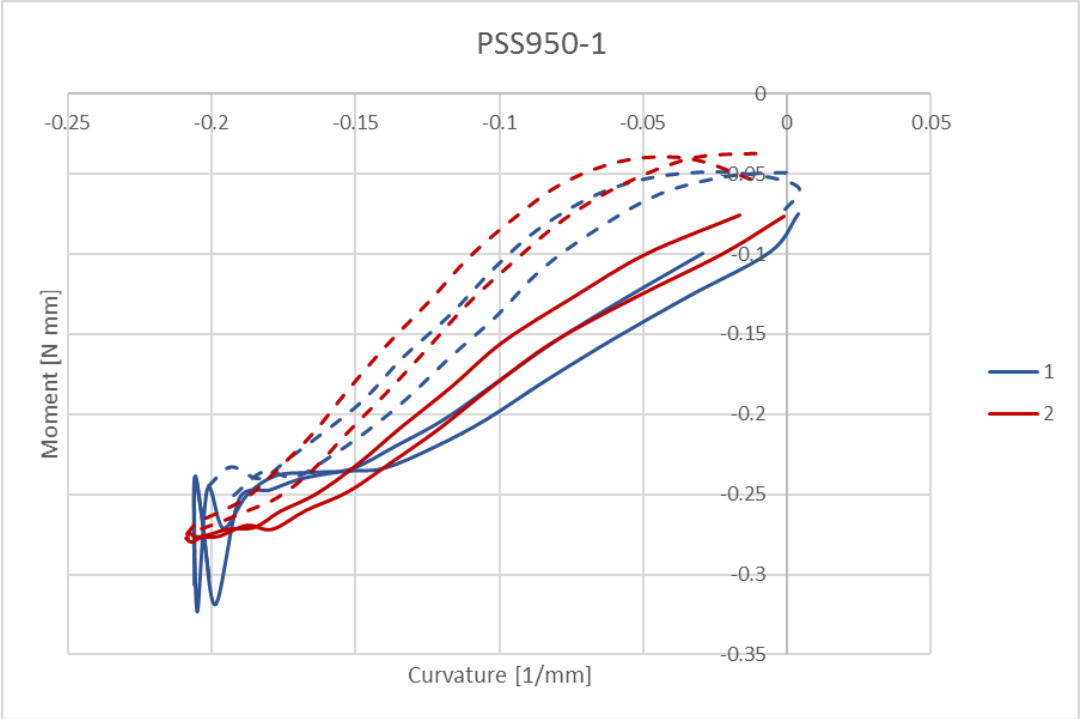

FIGURE 50. MOMENT VS. CURVATURE OF PLOTTED SMOOTH-SIL 950 SAMPLE (SOLID LOADING, DASHED UNLOADING)

5.3 – Discussion

From the results of the bending tests, it can be seen that the Smooth-Sil 950 hinge is stiffer than the Mold Star 30 hinges. This is expected as the Smooth-Sil 950 is much stiffer than the Mold Star 30, see Table 1. Additionally, the higher tear strength of the Smooth-Sil 950 prevents the silicone from being pulled away from the carbon fiber reinforcement as easily as the Mold Star 30, which could be an important consideration for deployable structure applications. The comparison between the hand fabricated and plotted Mold Star 30 samples is less clear, however. The average bending stiffness suggests that the plotted sample is stiffer than the hand fabricated sample, but it is difficult to make this conclusion since one coupon test yielded a significantly higher stiffness than the other two. If that data point is removed from the calculation of the average, the plotted sample appears to be less stiff. This implies that either one part of the sample was much stiffer than the others because of epoxy incursion into the hinge or there was a flaw in that particular test. Either way, it is necessary to conduct more tests to increase the accuracy of the results.

The stiffer hinges produced by the Smooth-Sil 950 result in higher strain energy storage within the composite than the Mold Star 30 hinges. Strain energy storage would be an important factor to consider when incorporating dual-matrix composites into self-deploying structures. For very large deployable structures or those deploying another mass, the energy required to fully deploy the structure would be higher than smaller, lighter structures. The hyperelastic matrix chosen for the hinges could allow for tuning of the strain energy storage depending on the application of the composite.

For some of the samples tested, Vic-3D 7 lost sight of the speckle pattern during certain parts of the test and therefore was unable to calculate the curvature across the entire hinge region. Coupon 3 from the PSS950-1 sample was the most severely affected to the point that there was not enough curvature data to calculate any information regarding bending stiffness. Further testing is required to increase sample size and improve the accuracy of the material properties gathered. Additionally, it would be beneficial to make efforts to ensure the samples

remain in the camera's focus and the speckle pattern is able to be tracked throughout the duration of the test.

5.4 – Conclusions

Dual-matrix composite samples were tested using a novel bending fixture that allows for a large range of motion of highly flexible composites and application of a near pure bending moment. Using compressive data from the load frame and deformation captured by 3D DIC the bending stiffness of the composite hinges was calculated. A stiffer matrix in the hinge region results in a higher bending stiffness, but it is still unclear if the fabrication method influences the bending stiffness of a simple hinge as well. Further testing is required to improve test procedures and increase accuracy of material properties.

Chapter 6 – Conclusions

6.1 – Dual-Matrix Composite Origami

Methods of infusing silicone through a two-step process to create discrete regions flexible and stiff matrices was explored and applied to complex origami hinge architectures. By bounding off hinge regions, infusing a flexible silicone matrix, and allowing it to cure before finally infusing a stiff matrix, structures with highly localized flexible hinges could be made. Several different traditional and modern origami designs from were fabricated to prove that dual-matrix composites can be implemented as structures with complex folding geometries. These fabrication techniques can be applied to manufacture lightweight, self-deploying structures such as booms and panels as well as high-performance mechanical metamaterials. However, the hand fabrication techniques were deemed too inconsistent and nonrepeatable to meet the demands of high accuracy and precision of the hinges of these complex structures, and a computer controlled solution was explored.

6.2 – CNC Plotter for Dual-Matrix Composites

A computer numerical control plotter was developed to meet the needs of dual-matrix composite fabrication. Computerized modeling of the hinge architectures and control of the silicone infusion process addresses the flaws exhibited by the hand fabrication methods by increasing both accuracy and repeatability of infusion. The plotter also greatly reduced both the material waste generated by the fabrication process and the infusion setup time by eliminating the need for the hinge bounding process. Origami hinge geometries were infused, and the resulting composites were folded into their alternate configurations. The plotter shows promise as a method to consistently produce the accurate hinge geometries required by highly complex origami deployable structures and mechanical metamaterials. The modular design of the plotter provides room for expansion as well as implementation of other flexible matrix materials.

6.3 – Dual-Matrix Composite Material Testing

Dual-matrix composite coupons were tested in bending using an Instron load frame equipped with a fixture specially designed to induce near pure bending while allowing for a large range of motion. During testing, samples were subjected to a 90° bend and returned to their original state at the end of the test. The bending stiffness was determined for each sample tested by using the bending moment determined from the compressive force data alongside curvature of the hinge gathered using a 3D DIC system. Stiffer silicone systems result in stiffer hinges, but there are also other properties, such as tear strength, that should be considered when selecting silicone resin systems.

6.3 – Future Work

With the silicone plotter capable of reliably producing accurate hinge geometries, it is important to fine tune the consistency of the final hinge. Adjustments will need to be made to the O-ring infuser so it will provide a more even infusion pressure as it passes over the uncured silicone. Additional resin systems should be tested in the plotter to determine how well it handles systems such as UV cure silicones and systems of lower and higher viscosities.

The plotter should be employed to fabricate much more complex hinge geometries. With its accuracy and repeatability, larger folding structures should be much easier to fabricate than before. A longer Miura tube should be manufactured to further test its feasibility as a deployable boom for space applications. Fabrication of mechanical metamaterials should also be explored to create high-performance transforming structures.

Testing should be continued to improve the accuracy of the results. More data points will give a more accurate representation of the material properties of dual-matrix composites and allow for improved modeling capabilities. Test methods should also be refined to produce more consistent results, especially when it comes to the curvature from DIC.

REFERENCES

[1] P. A. Warren, B. J. Dobson, J. D. Hinkle, and M. Silver, "Experimental Characterization of Lightweight Strain Energy Deployment Hinges," 46th AIAA/ASME/ASCE/AHS/ASC Structures, Structural Dynamics & Materials Conference, AIAA, Austin, TX, April 2005.

[2] B. E. Paton, L. M. Lovanov, V. S. Volkov, "Metal transformable-volume structures for space engineering," *Acta Astronautica*, Vol. 110, 2015, pp. 50-57.

[3] T. W. Murphey, W. H. Francis, B. L. Davis, J. Mejia-Ariza, M. Santer, J. N. Footdale, K. Schmid, O. Soykasap, K. Guidanean, and P. A. Warren, "High Strain Composites," 2nd AIAA Spacecraft Structures Conference, AIAA, Kissimmee, FL, January 2015.

[4] J. Block, M. Straubel, M. Wiedemann, "Ultralight deployable booms for solar sails and other large gossamer structures in space," *Acta Astronautica*, Vol. 68, 2011, pp. 984-992.

[5] H. M. Y. C. Mallikarachchi and S. Pellegrino, "Design of Ultrathin Composite Self-Deployable Booms," *Journal of Spacecraft and Rockets,* Vol. 51, No. 6, November-December 2014, pp. 1811-1821.

[6] F. L. Jiménez and S. Pellegrino, "Folding of fiber composites with a hyperelastic matrix," *International Journal of Solids and Structures,* Vol. 49, 2012, pp. 395-407.

[7] L. Datashvili, "Multifunctional and dimensionally stable flexible fibre composites for space applications," *Acta Astronautica,* Vol. 66, 2010, pp. 1081-1086.

[8] I. Maqueda, S. Pellegrino, and J. M. Mejia-Ariza, "Characterization of a high strain composite material," 53rd AIAA/ASME/ASCE/AHS/ASC Structures, Structural Dynamics, and Materials Conference, AIAA, Honolulu, HI, 2012.

[9] M. Sakovsky, S. Pellegrino, H. M. Y. C. Mallikarachchi, "Folding and Deployment of Closed Cross-Section Dual-Matrix Composite Booms," 3rd AIAA Spacecraft Structures Conference, AIAA SciTech Forum, 2016.

[10] M. Sakovsky, I. Maqueda, C. Karl, S. Pellegrino, and J. Costantine, " Dual-Matrix Composite Wideband Antenna Structures for CubeSats," 2nd AIAA Spacecraft Structures Conference, AIAA, Kissimmee, FL, January 2015.

[11] J. F. Sauder and B. Trease, "Deployment Testing of Flexible Composite Hinges in Bi-Material Beams," 3rd AIAA Spacecraft Structures Conference, AIAA, San Diego, CA, January 2016.

[12] M. Perez, "Origami-inspired Robot Can Hitch a Ride with a Rover," *NASA Jet Propulsion Laboratory,* NASA, March 20, 2017, web: https://www.nasa.gov/feature/jpl/origami-inspired-robot-can-hitch-a-ride-with-a-rover.

[13] R. B. Mulford, M. R. Jones, and B. D. Iverson, "Dynamic Control of Radiative Surface Properties With Origami-Inspired Design," *Journal of Heat Transfer,* Vol. 138, March 2016.

[14] K. Kuriki, K. Ninomiya, M. Nagatomo, N. Tsuya, M. Kawachi, K. Ijichi, and K. Himura, "The Design and Orbital Operation of Space Flyer Unit," *Acta Astronautica,* Vol. 24, 1991, pp. 33-43.

[15] K. Kuriki, K. Ninomiya, M. Takei, and S. Matsuoka, "Lessons Learned from the Space Flyer Unit (SFU) Mission," *Acta Astronautica,* Vol. 51, No. 11, 2002, pp 797-806.

[16] Y. Nishiyama, "Miura Folding: Applying Origami to Space Exploration," *International Journal of Pure and Applied Mathematics,* Vol. 79, No. 2, 2012, pp. 269-279.

[17] S. A. Zirbel, R. J. Lang, M. W. Thomson, D. A. Sigel, P. E. Walkemeyer, B. P. Trease, S. P. Magleby, and L. L. Howell, "Accommodating Thickness in Origami-Based Deployable Arrays," *Journal of Mechanical Design,* Vol. 135, November 2013.

[18] C. E. C. White, "Manufacturing and Structural Characterization of Flexible and Dual-Matrix Deployable Composites for Space Application," Master's thesis, North Carolina State University, Raleigh, North Carolina, 2016.

[19] M. Schenk and S. D. Guest, "Geometry of Miura-folded metamaterials," *Proceedings of the National Academy of Sciences of the United States of America,* Vol. 110, No. 9, February 26, 2013, pp. 3276-3281.

[20] K. C. Cheung, T. Tachi, S. Calisch, K. Miura, "Origami interleaved tube cellular materials," *Smart Materials and Structures,* Vol. 23, 2014.

[21] E. T. Filipov, T. Tachi, and G. H. Paulino, "Origami tubes assembled into stiff, yet reconfigurable structures and metamaterials," *Proceedings of the National Academy of*

Sciences of the United States of America, Vol. 112, no. 40, October 6, 2015, pp. 12321-12326.

[22] J. Firth, C. White, and M. Pankow, "Closed Cross Section Manufacturing of a Deployable Boom and Novel Method to Measure Laminate Bending Stiffness," unpublished, July 2017.

APPENDICES

Appendix A – Sprinter Configuration File for Silicone Plotter (Configuration.h)

```
#ifndef CONFIGURATION_H
#define CONFIGURATION_H

// BASIC SETTINGS: select your board type, thermistor type, axis scaling, and endstop
configuration

//// The following define selects which electronics board you have. Please choose
the one that matches your setup
// MEGA/RAMPS up to 1.2  = 3,
// RAMPS 1.3/1.4 = 33
// Gen6 = 5,
// Gen6 deluxe = 51
// Sanguinololu up to 1.1 = 6
// Sanguinololu 1.2 and above = 62
// Gen 7 @ 16MHZ only= 7
// Gen 7 @ 20MHZ only= 71
// Teensylu (at90usb) = 8
// Printrboard Rev. B (ATMEGA90USB1286) = 9
// Gen 3 Plus = 21
// gen 3  Monolithic Electronics = 22
// Gen3 PLUS for TechZone Gen3 Remix Motherboard = 23
#define MOTHERBOARD 62

//// Thermistor settings:
// 1 is 100k thermistor
// 2 is 200k thermistor
// 3 is mendel-parts thermistor
// 4 is 10k thermistor
// 5 is ParCan supplied 104GT-2 100K
// 6 is EPCOS 100k
// 7 is 100k Honeywell thermistor 135-104LAG-J01
#define THERMISTORHEATER 1
#define THERMISTORBED 1


//// Calibration variables
// X, Y, Z, E steps per unit - Metric Prusa Mendel with Wade extruder:
#define _AXIS_STEP_PER_UNIT {43.787, 43.787, 45, 4000}
//#define _AXIS_STEP_PER_UNIT {43.787, 43.787, 250}
// Metric Prusa Mendel with Makergear geared stepper extruder:
//#define _AXIS_STEP_PER_UNIT {80,80,3200/1.25,1380}
// MakerGear Hybrid Prusa Mendel:
// Z axis value is for .9 stepper(if you have 1.8 steppers for Z, you need to use
2272.7272)
//#define _AXIS_STEP_PER_UNIT {104.987, 104.987, 4545.4544, 1487}


//// Endstop Settings
#define ENDSTOPPULLUPS // Comment this out (using // at the start of the line) to
disable the endstop pullup resistors
// The pullups are needed if you directly connect a mechanical endswitch between the
signal and ground pins.
//If your axes are only moving in one direction, make sure the endstops are connected
properly.
```

```
//If your axes move in one direction ONLY when the endstops are triggered, set
[XYZ]_ENDSTOP_INVERT to true here:
const bool X_ENDSTOP_INVERT = true;
const bool Y_ENDSTOP_INVERT = true;
const bool Z_ENDSTOP_INVERT = true;

// This determines the communication speed of the printer
#define BAUDRATE 115200
//#define BAUDRATE 250000

// Comment out (using // at the start of the line) to disable SD support:
//#define SDSUPPORT

// Uncomment to make run init.g from SD on boot
//#define SDINITFILE

//Only work with Atmega1284 you need +1 kb ram
//#define SD_FAST_XFER_AKTIV

//===========================================================================
//// STORE SETTINGS TO EEPROM
//===========================================================================
// the microcontroller can store settings in the EEPROM
// M500 - stores paramters in EEPROM
// M501 - reads parameters from EEPROM (if you need reset them after you changed them
temporarily).
// M502 - reverts to the default "factory settings". You still need to store them in
EEPROM afterwards if you want to.
// M503 - Print settings
// define this to enable eeprom support
//#define USE_EEPROM_SETTINGS

// to disable EEPROM Serial responses and decrease program space by ~1000 byte:
comment this out:
// please keep turned on if you can.
//#define PRINT_EEPROM_SETTING

//===========================================================================
//// ARC Function (G2/G3 Command)
//===========================================================================
//Uncomment to aktivate the arc (circle) function (G2/G3 Command)
//Without SD function an ARC function the used Flash is smaller 31 kb
#define USE_ARC_FUNCTION

//===========================================================================
//// ADVANCED SETTINGS - to tweak parameters
//===========================================================================

#ifdef SDSUPPORT
      #ifdef SD_FAST_XFER_AKTIV
            //Fast transfer chunk size (> 1024 is unstable, change at your own
risk).
            #define SD_FAST_XFER_CHUNK_SIZE 1024
      #endif
#endif

//===========================================================================
// For Inverting Stepper Enable Pins (Active Low) use 0, Non Inverting (Active High)
use 1
```

```
//===========================================================================
#define X_ENABLE_ON 0
#define Y_ENABLE_ON 0
#define Z_ENABLE_ON 0
#define E_ENABLE_ON 0

//Uncomment if you have problems with a stepper driver enabeling too late, this will
also set how many microseconds delay there will be after enabeling the driver
//#define DELAY_ENABLE 15

//===========================================================================
// Disables axis when it's not being used.
//===========================================================================
const bool DISABLE_X = false;
const bool DISABLE_Y = false;
const bool DISABLE_Z = true;
const bool DISABLE_E = false;

//===========================================================================
// Inverting axis direction
//===========================================================================
const bool INVERT_X_DIR = true;
const bool INVERT_Y_DIR = false;
const bool INVERT_Z_DIR = true;
const bool INVERT_E_DIR = false;

//===========================================================================
//// ENDSTOP SETTINGS:
//===========================================================================
// Sets direction of endstops when homing; 1=MAX, -1=MIN
#define X_HOME_DIR -1
#define Y_HOME_DIR -1
#define Z_HOME_DIR -1

//#define ENDSTOPS_ONLY_FOR_HOMING // If defined the endstops will only be used for
homing

const bool min_software_endstops = false; //If true, axis won't move to coordinates
less than zero.
const bool max_software_endstops = true; //If true, axis won't move to coordinates
greater than the defined lengths below.


//===========================================================================
//Max Length for Prusa Mendel, check the ways of your axis and set this Values
//===========================================================================
const int X_MAX_LENGTH = 640;
const int Y_MAX_LENGTH = 600;
const int Z_MAX_LENGTH = 10;

//===========================================================================
//// MOVEMENT SETTINGS
//===========================================================================
const int NUM_AXIS = 4; // The axis order in all axis related arrays is X, Y, Z, E
//const int NUM_AXIS = 3; // The axis order in all axis related arrays is X, Y, Z, E
#define _MAX_FEEDRATE {25, 25, 25, 10}       // (mm/sec)
#define _HOMING_FEEDRATE {1500,1500,1500}      // (mm/min) !!
#define _AXIS_RELATIVE_MODES {false, false, false, false}
//#define _MAX_FEEDRATE {25, 25, 45}       // (mm/sec)
```

```
//#define _HOMING_FEEDRATE {1500,1500}      // (mm/min) !!
//#define _AXIS_RELATIVE_MODES {false, false, false}

#define MAX_STEP_FREQUENCY 30000 // Max step frequency

//For the retract (negative Extruder) move this maxiumum Limit of Feedrate is used
//The next positive Extruder move use also this Limit,
//then for the next (second after retract) move the original Maximum (_MAX_FEEDRATE)
Limit is used
#define MAX_RETRACT_FEEDRATE 50    //mm/sec

//------------------------------------------------------------------------
//// Not used at the Moment
//------------------------------------------------------------------------

// Min step delay in microseconds. If you are experiencing missing steps, try to
raise the delay microseconds, but be aware this
// If you enable this, make sure STEP_DELAY_RATIO is disabled.
//#define STEP_DELAY_MICROS 1

// Step delay over interval ratio. If you are still experiencing missing steps, try
to uncomment the following line, but be aware this
// If you enable this, make sure STEP_DELAY_MICROS is disabled. (except for Gen6:
both need to be enabled.)
//#define STEP_DELAY_RATIO 0.25

///Oscillation reduction.  Forces x,y,or z axis to be stationary for ## ms before
allowing axis to switch direcitons.  Alternative method to prevent skipping steps.
Uncomment the line below to activate.
// At this Version with Planner this Function ist not used
//#define RAPID_OSCILLATION_REDUCTION

#ifdef RAPID_OSCILLATION_REDUCTION
const long min_time_before_dir_change = 30; //milliseconds
#endif

//------------------------------------------------------------------------
//// Acceleration settings
//------------------------------------------------------------------------
// X, Y, Z, E maximum start speed for accelerated moves. E default values are good
for skeinforge 40+, for older versions raise them a lot.
#define _ACCELERATION 25         // Axis Normal acceleration mm/s^2
#define _RETRACT_ACCELERATION 25 // Extruder Normal acceleration mm/s^2
#define _MAX_XY_JERK 20.0
#define _MAX_Z_JERK 0.4
#define _MAX_E_JERK 5.0    // (mm/sec)
//#define _MAX_START_SPEED_UNITS_PER_SECOND {25.0,25.0,0.2,10.0}
#define _MAX_ACCELERATION_UNITS_PER_SQ_SECOND {50,50,50,30}    // X, Y, Z and E max
acceleration in mm/s^2 for printing moves or retracts


// Minimum planner junction speed. Sets the default minimum speed the planner plans
for at the end
// of the buffer and all stops. This should not be much greater than zero and should
only be changed
// if unwanted behavior is observed on a user's machine when running at very slow
speeds.
#define MINIMUM_PLANNER_SPEED 0.05 // (mm/sec)
```

```
#define DEFAULT_MINIMUMFEEDRATE       0.0     // minimum feedrate
#define DEFAULT_MINTRAVELFEEDRATE     0.0

#define _MIN_SEG_TIME 20000

// If defined the movements slow down when the look ahead buffer is only half full
#define SLOWDOWN


const int dropsegments=5; //everything with less than this number of steps will be
ignored as move and joined with the next movement

//===========================================================================
// Machine UUID
//===========================================================================
// This may be useful if you have multiple machines and wish to identify them by
using the M115 command.
// By default we set it to zeros.
#define _DEF_CHAR_UUID "00000000-0000-0000-0000-000000000000"



//===========================================================================
//// Planner buffer Size
//===========================================================================

// The number of linear motions that can be in the plan at any give time
// if the SD Card need to much memory reduce the Values for Plannerpuffer (base of
2)
#ifdef SDSUPPORT
  #define BLOCK_BUFFER_SIZE 16
  #define BLOCK_BUFFER_MASK 0x0f
#else
  #define BLOCK_BUFFER_SIZE 16
  #define BLOCK_BUFFER_MASK 0x0f
#endif

//===========================================================================
//// SETTINGS FOR ARC FUNCTION (Command G2/G2)
//===========================================================================

// Arc interpretation settings:
//Step to split a cirrcle in small Lines
#define MM_PER_ARC_SEGMENT 1
//After this count of steps a new SIN / COS caluclation is startet to correct the
circle interpolation
#define N_ARC_CORRECTION 25

//===========================================================================
//// FANCONTROL WITH SOFT PWM
//===========================================================================

//With this option its possible to drive the fan with SOFT PWM (500hz) and use
//every Digital output for it, main usage for Sanguinololu
#define FAN_SOFT_PWM

//===========================================================================
//// MINIMUM START SPEED FOR FAN
//===========================================================================
```

```
//Minimum start speed for FAN when the last speed was zero
//Set to 0 to deaktivate
//If value is set the fan will drive with this minimum speed for
MINIMUM_FAN_START_TIME
#define MINIMUM_FAN_START_SPEED  0

//This is the time how long the minimum FAN speed is set
#define MINIMUM_FAN_START_TIME  6000    //6sec

//------------------------------------------------------------------------
//// HEATERCONTROL AND PID PARAMETERS
//------------------------------------------------------------------------

//Testfunction to adjust the Hotend temperatur in case of Printingspeed
//If the Printer print slow the Temp is going to AUTO_TEMP_MIN
//At the moment this Value dont change the targettemp from the Hotend
//The result of this function is only send with the Temperaturerequest to the host
//#define AUTOTEMP
#ifdef AUTOTEMP
    #define AUTO_TEMP_MAX 240
    #define AUTO_TEMP_MIN 205
    #define AUTO_TEMP_FACTOR 0.025
    #define AUTOTEMP_OLDWEIGHT 0.98
#endif

//// AD595 THERMOCOUPLE SUPPORT UNTESTED... USE WITH CAUTION!!!!

//// PID settings:
// Uncomment the following line to enable PID support. This is untested and could be
disastrous. Be careful.
#define PIDTEMP 1
#ifdef PIDTEMP
//Sanguinololu 1.2 and above, the PWM Output Hotend Timer 1 is used for the Hardware
PWM
//but in this Software use Timer1 for the Stepperfunction so it is not possible to
use the "analogWrite" function.
//This Soft PWM use Timer 2 with 400 Hz to drive the PWM for the hotend
#define PID_SOFT_PWM

//Measure the MIN/MAX Value of the Hotend Temp and show it with
//Command M601 / Command M602 Reset the MIN/MAX Value
//#define DEBUG_HEATER_TEMP

// M303 - PID relay autotune S<temperature> sets the target temperature.
// (default target temperature = 150C)
#define PID_AUTOTUNE

//PID Controler Settings
#define PID_INTEGRAL_DRIVE_MAX 80 // too big, and heater will lag after changing
temperature, too small and it might not compensate enough for long-term errors
#define PID_PGAIN 2560 //256 is 1.0  // value of X means that error of 1 degree is
changing PWM duty by X, probably no need to go over 25
#define PID_IGAIN 64 //256 is 1.0  // value of X (e.g 0.25) means that each degree
error over 1 sec (2 measurements) changes duty cycle by 2X (=0.5) units (verify?)
#define PID_DGAIN 4096 //256 is 1.0  // value of X means that around reached setpoint,
each degree change over one measurement (half second) adjusts PWM by X units to
compensate
```

```
// magic formula 1, to get approximate "zero error" PWM duty. Take few measurements with low PWM duty and make linear fit to get the formula
//        for        my        makergear        hot-end:        linear        fit {50,10},{60,20},{80,30},{105,50},{176,100},{128,64},{208,128}
#define HEATER_DUTY_FOR_SETPOINT(setpoint) ((int)((187L*(long)setpoint)>>8)-27)
// magic formula 2, to make led brightness approximately linear
#define LED_PWM_FOR_BRIGHTNESS(brightness) ((64*brightness-1384)/(300-brightness))
#endif

// Change this value (range 30-255) to limit the current to the nozzle
#define HEATER_CURRENT 255

// How often should the heater check for new temp readings, in milliseconds
#define HEATER_CHECK_INTERVAL 500
#define BED_CHECK_INTERVAL 5000

// Comment the following line to enable heat management during acceleration
#define DISABLE_CHECK_DURING_ACC
#ifndef DISABLE_CHECK_DURING_ACC
  // Uncomment the following line to disable heat management during moves
  //#define DISABLE_CHECK_DURING_MOVE
#endif

// Uncomment the following line to disable heat management during travel moves (and extruder-only moves, eg: retracts), strongly recommended if you are missing steps mid print.
// Probably this should remain commented if are using PID.
// It also defines the max milliseconds interval after which a travel move is not considered so for the sake of this feature.
#define DISABLE_CHECK_DURING_TRAVEL 1000

//// Temperature smoothing - only uncomment this if your temp readings are noisy (Gen6 without EvdZ's 5V hack)
//#define SMOOTHING
//#define SMOOTHFACTOR 16 //best to use a power of two here - determines how many values are averaged together by the smoothing algorithm


//// Experimental watchdog and minimal temp
// The watchdog waits for the watchperiod in milliseconds whenever an M104 or M109 increases the target temperature
// If the temperature has not increased at the end of that period, the target temperature is set to zero. It can be reset with another M104/M109
//#define WATCHPERIOD 5000 //5 seconds

// Actual temperature must be close to target for this long before M109 returns success
//#define TEMP_RESIDENCY_TIME 20  // (seconds)
//#define TEMP_HYSTERESIS 5      // (C°) range of +/- temperatures considered "close" to the target one

//// The minimal temperature defines the temperature below which the heater will not be enabled
#define MINTEMP 5

//// Experimental max temp
// When temperature exceeds max temp, your heater will be switched off.
// This feature exists to protect your hotend from overheating accidentally, but *NOT* from thermistor short/failure!
```

```
// You should use MINTEMP for thermistor short/failure protection.
#define MAXTEMP 275

// Select one of these only to define how the nozzle temp is read.
#define HEATER_USES_THERMISTOR
//#define HEATER_USES_AD595
//#define HEATER_USES_MAX6675

// Select one of these only to define how the bed temp is read.
#define BED_USES_THERMISTOR
//#define BED_USES_AD595

//This is for controlling a fan to cool down the stepper drivers
//it will turn on when any driver is enabled
//and turn off after the set amount of seconds from last driver being disabled again
//#define CONTROLLERFAN_PIN 23 //Pin used for the fan to cool controller, comment
out to disable this function
#define CONTROLLERFAN_SEC 60 //How many seconds, after all motors were disabled, the
fan should run

//This is for controlling a fan that will keep the extruder cool.
//#define EXTRUDERFAN_PIN 66 //Pin used to control the fan, comment out to disable
this function
#define EXTRUDERFAN_DEC 50 //Hotend temperature from where the fan will be turned on

//#define CHAIN_OF_COMMAND 1 //Finish buffered moves before executing M42, fan speed,
heater target, and so...

//===========================================================================
// DEBUGING
//===========================================================================


//Uncomment this to see on the host if a wrong or unknown Command is recived
//Only for Testing !!!
//#define SEND_WRONG_CMD_INFO

// Uncomment the following line to enable debugging. You can better control debugging
below the following line
//#define DEBUG
#ifdef DEBUG
  //#define DEBUG_PREPARE_MOVE //Enable this to debug prepare_move() function
  //#define DEBUG_MOVE_TIME //Enable this to time each move and print the result
  //#define DEBUG_HEAT_MGMT //Enable this to debug heat management. WARNING, this
will cause axes to jitter!
  //#define DEBUG_DISABLE_CHECK_DURING_TRAVEL //Debug the namesake feature, see above
in this file
#endif

#endif
```

Appendix B – Slic3r Configuration Bundle for Silicone Plotter

```
# generated by Slic3r 1.3.0-dev on Mon Jul 24 14:23:56 2017

[filament:Simple Mode]
bed_temperature = 0
bridge_fan_speed = 100
compatible_printers =
cooling = 1
disable_fan_first_layers = 3
end_filament_gcode = "; Filament-specific end gcode \n;END gcode for filament\n"
extrusion_multiplier = 1
fan_always_on = 0
fan_below_layer_time = 60
filament_colour = #FFFFFF
filament_cost = 0
filament_density = 0
filament_diameter = 23
filament_max_volumetric_speed = 0
filament_notes = ""
filament_settings_id =
first_layer_bed_temperature = 0
first_layer_temperature = 66
max_fan_speed = 100
min_fan_speed = 35
min_print_speed = 10
slowdown_below_layer_time = 5
start_filament_gcode = "; Filament gcode\n"
temperature = 66

[filament:silicone]
bed_temperature = 0
bridge_fan_speed = 100
compatible_printers =
cooling = 1
disable_fan_first_layers = 3
end_filament_gcode = "; Filament-specific end gcode \n;END gcode for filament\n"
extrusion_multiplier = 1.1
fan_always_on = 0
fan_below_layer_time = 60
filament_colour = #28C1FB
filament_cost = 0
filament_density = 0
filament_diameter = 23
filament_max_volumetric_speed = 0
filament_notes = ""
filament_settings_id =
first_layer_bed_temperature = 0
first_layer_temperature = 66
max_fan_speed = 100
min_fan_speed = 35
min_print_speed = 10
slowdown_below_layer_time = 5
start_filament_gcode = "; Filament gcode\n"
temperature = 66
```

```
[presets]
filament = silicone
print = silicone
printer = silicone

[print:Simple Mode]
avoid_crossing_perimeters = 0
bottom_infill_pattern = rectilinear
bottom_solid_layers = 3
bridge_acceleration = 0
bridge_flow_ratio = 1
bridge_speed = 60
brim_connections_width = 0
brim_width = 0
compatible_printers =
complete_objects = 0
default_acceleration = 0
dont_support_bridges = 1
external_perimeter_extrusion_width = 0
external_perimeter_speed = 50%
external_perimeters_first = 0
extra_perimeters = 1
extruder_clearance_height = 20
extruder_clearance_radius = 20
extrusion_width = 0
fill_angle = 45
fill_density = 40%
fill_gaps = 1
fill_pattern = honeycomb
first_layer_acceleration = 0
first_layer_extrusion_width = 200%
first_layer_height = 0.35
first_layer_speed = 30
gap_fill_speed = 20
gcode_comments = 0
infill_acceleration = 0
infill_every_layers = 1
infill_extruder = 1
infill_extrusion_width = 0
infill_first = 0
infill_only_where_needed = 0
infill_overlap = 55%
infill_speed = 60
interface_shells = 0
interior_brim_width = 0
layer_height = 1.9
max_print_speed = 80
max_volumetric_speed = 0
min_skirt_length = 0
notes =
only_retract_when_crossing_perimeters = 1
ooze_prevention = 0
output_filename_format = [input_filename_base].gcode
overhangs = 1
overridable = support_material
perimeter_acceleration = 0
perimeter_extruder = 1
perimeter_extrusion_width = 0
perimeter_speed = 30
```

```
perimeters = 3
post_process =
print_settings_id =
raft_layers = 0
resolution = 0
seam_position = aligned
skirt_distance = 6
skirt_height = 1
skirts = 1
small_perimeter_speed = 15
solid_infill_below_area = 70
solid_infill_every_layers = 0
solid_infill_extruder = 1
solid_infill_extrusion_width = 0
solid_infill_speed = 20
spiral_vase = 0
standby_temperature_delta = -5
support_material = 0
support_material_angle = 0
support_material_buildplate_only = 0
support_material_contact_distance = 0.2
support_material_enforce_layers = 0
support_material_extruder = 1
support_material_extrusion_width = 0
support_material_interface_extruder = 1
support_material_interface_layers = 3
support_material_interface_spacing = 0
support_material_interface_speed = 100%
support_material_pattern = pillars
support_material_spacing = 2.5
support_material_speed = 60
support_material_threshold = 60%
thin_walls = 1
top_infill_extrusion_width = 0
top_infill_pattern = rectilinear
top_solid_infill_speed = 15
top_solid_layers = 3
travel_speed = 130
xy_size_compensation = 0

[print:silicone]
avoid_crossing_perimeters = 1
bottom_infill_pattern = rectilinear
bottom_solid_layers = 3
bridge_acceleration = 0
bridge_flow_ratio = 1
bridge_speed = 60
brim_connections_width = 0
brim_width = 0
compatible_printers =
complete_objects = 0
default_acceleration = 0
dont_support_bridges = 1
external_perimeter_extrusion_width = 0
external_perimeter_speed = 50%
external_perimeters_first = 0
extra_perimeters = 0
extruder_clearance_height = 20
extruder_clearance_radius = 20
```

```
extrusion_width = 0
fill_angle = 45
fill_density = 40%
fill_gaps = 1
fill_pattern = honeycomb
first_layer_acceleration = 0
first_layer_extrusion_width = 200%
first_layer_height = 0.35
first_layer_speed = 100%
gap_fill_speed = 20
gcode_comments = 0
infill_acceleration = 0
infill_every_layers = 1
infill_extruder = 1
infill_extrusion_width = 0
infill_first = 0
infill_only_where_needed = 0
infill_overlap = 55%
infill_speed = 40
interface_shells = 0
interior_brim_width = 0
layer_height = 0.3
max_print_speed = 80
max_volumetric_speed = 0
min_skirt_length = 0
notes =
only_retract_when_crossing_perimeters = 1
ooze_prevention = 0
output_filename_format = [input_filename_base].gcode
overhangs = 0
overridable = support_material
perimeter_acceleration = 0
perimeter_extruder = 1
perimeter_extrusion_width = 0
perimeter_speed = 40
perimeters = 3
post_process =
print_settings_id =
raft_layers = 0
resolution = 0
seam_position = nearest
skirt_distance = 10
skirt_height = 1
skirts = 0
small_perimeter_speed = 15
solid_infill_below_area = 70
solid_infill_every_layers = 0
solid_infill_extruder = 1
solid_infill_extrusion_width = 0
solid_infill_speed = 20
spiral_vase = 0
standby_temperature_delta = -5
support_material = 0
support_material_angle = 0
support_material_buildplate_only = 0
support_material_contact_distance = 0.2
support_material_enforce_layers = 0
support_material_extruder = 1
support_material_extrusion_width = 0
```

```
support_material_interface_extruder = 1
support_material_interface_layers = 3
support_material_interface_spacing = 0
support_material_interface_speed = 100%
support_material_pattern = pillars
support_material_spacing = 2.5
support_material_speed = 60
support_material_threshold = 60%
thin_walls = 0
top_infill_extrusion_width = 0
top_infill_pattern = rectilinear
top_solid_infill_speed = 15
top_solid_layers = 3
travel_speed = 130
xy_size_compensation = 0

[printer:Simple Mode]
bed_shape = 0x0,720x0,720x700,0x700
before_layer_gcode =
between_objects_gcode =
end_gcode = M104 S0 ; turn off temperature\nG28 X0  ; home X axis\nM84     ;
disable motors\n
extruder_offset = 0x0
gcode_flavor = reprap
has_heatbed = 1
layer_gcode =
notes =
nozzle_diameter = 1.25
octoprint_apikey =
octoprint_host =
pressure_advance = 0
printer_notes = ""
printer_settings_id =
retract_before_travel = 2
retract_layer_change = 0
retract_length = 1
retract_length_toolchange = 10
retract_lift = 0
retract_lift_above = 0
retract_lift_below = 0
retract_restart_extra = 0
retract_restart_extra_toolchange = 0
retract_speed = 40
serial_port =
serial_speed = 250000
start_gcode = G28 ; home all axes\nG1 Z5 F5000 ; lift nozzle\n
toolchange_gcode =
use_firmware_retraction = 0
use_relative_e_distances = 0
use_volumetric_e = 0
vibration_limit = 0
wipe = 0
z_offset = 0
z_steps_per_mm = 0

[printer:silicone]
bed_shape = 0x0,640x0,640x600,0x600
before_layer_gcode =
between_objects_gcode =
```

```
end_gcode = M104 S0 ; turn off temperature\nM84     ; disable motors\n
extruder_offset = 0x0
gcode_flavor = reprap
has_heatbed = 0
layer_gcode =
notes =
nozzle_diameter = 1.25
octoprint_apikey =
octoprint_host =
pressure_advance = 0
printer_notes = ""
printer_settings_id =
retract_before_travel = 2
retract_layer_change = 0
retract_length = 0
retract_length_toolchange = 10
retract_lift = 0
retract_lift_above = 0
retract_lift_below = 0
retract_restart_extra = 0
retract_restart_extra_toolchange = 0
retract_speed = 40
serial_port =
serial_speed = 250000
start_gcode = G28 X0 Y0 ; home x&y axes\n
toolchange_gcode =
use_firmware_retraction = 0
use_relative_e_distances = 0
use_volumetric_e = 0
vibration_limit = 0
wipe = 0
z_offset = 0
z_steps_per_mm = 0

[settings]
autocenter = 1
```

Appendix C – G-code for blintz hinge model

```
; generated by Slic3r 1.3.0-dev on 2017-07-21 at 16:04:37

; external perimeters extrusion width = 1.25mm (7.11mm^3/s)
; perimeters extrusion width = 2.13mm (24.73mm^3/s)
; infill extrusion width = 3.75mm (44.23mm^3/s)
; solid infill extrusion width = 2.13mm (12.36mm^3/s)
; top infill extrusion width = 2.13mm (9.27mm^3/s)

M107
M104 S66 ; set temperature
G28 X0 Y0 ; home x&y axes

; Filament gcode

M109 S66 ; set temperature and wait for it to be reached
G21 ; set units to millimeters
G90 ; use absolute coordinates
M82 ; use absolute distances for extrusion
G92 E0
G1 Z0.350 F7800.000
G1 X319.725 Y300.664 F7800.000
G1 F2400
G1 X319.725 Y449.336 E0.08609
G1 X245.389 Y375.000 E0.14696
G1 X319.592 Y300.797 E0.20773
G1 X319.100 Y302.173 F7800.000
G1 F1200
G1 X319.100 Y447.827 E0.29207
G1 X246.273 Y375.000 E0.35171
G1 X318.967 Y302.305 E0.41124
G1 X320.307 Y301.849 F7800.000
G92 E0
G1 X320.275 Y299.336 F7800.000
G1 F2400
G1 X320.275 Y150.664 E0.08609
G1 X394.611 Y225.000 E0.14696
G1 X320.408 Y299.203 E0.20773
G1 X320.900 Y297.827 F7800.000
G1 F1200
G1 X320.900 Y152.173 E0.29207
G1 X393.727 Y225.000 E0.35171
G1 X321.033 Y297.695 E0.41124
G1 X319.817 Y298.452 F7800.000
G92 E0
G1 X320.389 Y300.000 F7800.000
```

```
G1 F2400
G1 X395.000 Y225.389 E0.06110
G1 X469.611 Y300.000 E0.12220
G1 X395.000 Y374.611 E0.18330
G1 X320.522 Y300.133 E0.24429
G1 X321.273 Y300.000 F7800.000
G1 F1200
G1 X395.000 Y226.273 E0.30466
G1 X468.727 Y300.000 E0.36504
G1 X395.000 Y373.727 E0.42542
G1 X321.405 Y300.133 E0.48568
G1 X320.190 Y299.375 F7800.000
G1 X319.611 Y300.000 F7800.000
G1 F2400
G1 X245.000 Y374.611 E0.54678
G1 X170.389 Y300.000 E0.60788
G1 X245.000 Y225.389 E0.66898
G1 X319.478 Y299.867 E0.72997
G1 X318.727 Y300.000 F7800.000
G1 F1200
G1 X245.000 Y373.727 E0.79035
G1 X171.273 Y300.000 E0.85072
G1 X245.000 Y226.273 E0.91110
G1 X318.595 Y299.867 E0.97136
G1 X319.652 Y300.841 F7800.000
G1 X319.725 Y299.336 F7800.000
G1 F2400
G1 X245.389 Y225.000 E1.03224
G1 X319.725 Y150.664 E1.09311
G1 X319.725 Y299.148 E1.17909
G1 X319.100 Y297.827 F7800.000
G1 F1200
G1 X246.273 Y225.000 E1.23873
G1 X319.100 Y152.173 E1.29837
G1 X319.100 Y297.640 E1.38260
G1 X318.477 Y298.911 F7800.000
G92 E0
G1 X320.275 Y300.664 F7800.000
G1 F2400
G1 X394.611 Y375.000 E0.06087
G1 X320.275 Y449.336 E0.12175
G1 X320.275 Y300.852 E0.20773
G1 X320.900 Y302.173 F7800.000
G1 F1200
G1 X393.727 Y375.000 E0.26737
G1 X320.900 Y447.827 E0.32701
G1 X320.900 Y302.360 E0.41124
G1 X321.224 Y300.965 F7800.000
```

```
G92 E0
G1 X395.000 Y375.389 F7800.000
G1 F2400
G1 X320.000 Y450.389 E0.06142
G1 X245.000 Y375.389 E0.12284
G1 X170.884 Y449.505 E0.18353
G1 X170.495 Y449.116 E0.18385
G1 X244.611 Y375.000 E0.24454
G1 X169.611 Y300.000 E0.30596
G1 X244.611 Y225.000 E0.36738
G1 X170.495 Y150.884 E0.42807
G1 X170.884 Y150.495 E0.42839
G1 X245.000 Y224.611 E0.48908
G1 X320.000 Y149.611 E0.55050
G1 X395.000 Y224.611 E0.61192
G1 X469.116 Y150.495 E0.67261
G1 X469.505 Y150.884 E0.67293
G1 X395.389 Y225.000 E0.73363
G1 X470.389 Y300.000 E0.79504
G1 X395.389 Y375.000 E0.85646
G1 X469.505 Y449.116 E0.91716
G1 X469.116 Y449.505 E0.91748
G1 X395.133 Y375.522 E0.97806
G1 X395.000 Y376.273 F7800.000
G1 F1200
G1 X320.000 Y451.273 E1.03948
G1 X245.000 Y376.273 E1.10090
G1 X170.884 Y450.389 E1.16159
G1 X169.611 Y449.116 E1.16263
G1 X243.727 Y375.000 E1.22333
G1 X168.727 Y300.000 E1.28474
G1 X243.727 Y225.000 E1.34616
G1 X169.611 Y150.884 E1.40686
G1 X170.884 Y149.611 E1.40790
G1 X245.000 Y223.727 E1.46859
G1 X320.000 Y148.727 E1.53001
G1 X395.000 Y223.727 E1.59143
G1 X469.116 Y149.611 E1.65212
G1 X470.389 Y150.884 E1.65316
G1 X396.273 Y225.000 E1.71386
G1 X471.273 Y300.000 E1.77528
G1 X396.273 Y375.000 E1.83669
G1 X470.389 Y449.116 E1.89739
G1 X469.116 Y450.389 E1.89843
G1 X395.133 Y376.405 E1.95902
G1 X394.111 Y375.394 F7800.000
G1 Z0.650 F7800.000
G92 E0
```

```
G1 X319.375 Y448.491 F7800.000
G1 F1200
G1 X245.884 Y375.000 E0.09787
G1 X319.375 Y301.509 E0.19575
G1 X319.375 Y448.304 E0.33398
G1 X318.753 Y449.576 F7800.000
G92 E0
G1 X320.625 Y298.491 F7800.000
G1 F1200
G1 X320.625 Y151.509 E0.13841
G1 X394.116 Y225.000 E0.23629
G1 X320.758 Y298.359 E0.33398
G1 X319.542 Y299.116 F7800.000
G1 X320.884 Y300.000 F7800.000
G1 F1200
G1 X395.000 Y225.884 E0.43269
G1 X469.116 Y300.000 E0.53139
G1 X395.000 Y374.116 E0.63010
G1 X321.016 Y300.133 E0.72863
G1 X319.801 Y299.375 F7800.000
G92 E0
G1 X319.375 Y298.491 F7800.000
G1 F1200
G1 X245.884 Y225.000 E0.09787
G1 X319.375 Y151.509 E0.19575
G1 X319.375 Y298.304 E0.33398
G1 X318.753 Y299.575 F7800.000
G1 X319.116 Y300.000 F7800.000
G1 F1200
G1 X245.000 Y374.116 E0.43269
G1 X170.884 Y300.000 E0.53139
G1 X245.000 Y225.884 E0.63010
G1 X318.984 Y299.867 E0.72863
G1 X320.106 Y300.763 F7800.000
G92 E0
G1 X320.625 Y301.509 F7800.000
G1 F1200
G1 X394.116 Y375.000 E0.09787
G1 X320.625 Y448.491 E0.19575
G1 X320.625 Y301.696 E0.33398
G1 X320.949 Y300.301 F7800.000
G92 E0
G1 X395.000 Y375.884 F7800.000
G1 F1200
G1 X320.000 Y450.884 E0.09988
G1 X245.000 Y375.884 E0.19977
G1 X170.884 Y450.000 E0.29847
G1 X170.000 Y449.116 E0.29965
```

```
G1 X244.116 Y375.000 E0.39835
G1 X169.116 Y300.000 E0.49824
G1 X244.116 Y225.000 E0.59812
G1 X170.000 Y150.884 E0.69682
G1 X170.884 Y150.000 E0.69800
G1 X245.000 Y224.116 E0.79671
G1 X320.000 Y149.116 E0.89659
G1 X395.000 Y224.116 E0.99647
G1 X469.116 Y150.000 E1.09518
G1 X470.000 Y150.884 E1.09635
G1 X395.884 Y225.000 E1.19506
G1 X470.884 Y300.000 E1.29494
G1 X395.884 Y375.000 E1.39483
G1 X470.000 Y449.116 E1.49353
G1 X469.116 Y450.000 E1.49471
G1 X395.133 Y376.016 E1.59324
G1 X394.113 Y375.004 F7800.000
G92 E0
; Filament-specific end gcode
;END gcode for filament

M104 S0 ; turn off temperature
G28 X0  ; home X axis
M84     ; disable motors

; filament used = 8.3mm (3.4cm3)
; total filament cost = 0.0

; avoid_crossing_perimeters = 1
; bed_shape = 0x0,640x0,640x600,0x600
; bed_temperature = 0
; before_layer_gcode =
; between_objects_gcode =
; bridge_acceleration = 0
; bridge_fan_speed = 100
; brim_connections_width = 0
; brim_width = 0
; complete_objects = 0
; cooling = 1
; default_acceleration = 0
; disable_fan_first_layers = 3
; duplicate_distance = 6
; end_filament_gcode = "; Filament-specific end gcode \n;END gcode
for filament\n"
; end_gcode = M104 S0 ; turn off temperature\nG28 X0  ; home X
axis\nM84     ; disable motors\n
; extruder_clearance_height = 20
; extruder_clearance_radius = 20
```

```
; extruder_offset = 0x0
; extrusion_axis = E
; extrusion_multiplier = 1.1
; fan_always_on = 0
; fan_below_layer_time = 60
; filament_colour = #28C1FB
; filament_cost = 0
; filament_density = 0
; filament_diameter = 23
; filament_max_volumetric_speed = 0
; filament_notes = ""
; first_layer_acceleration = 0
; first_layer_bed_temperature = 0
; first_layer_extrusion_width = 200%
; first_layer_speed = 100%
; first_layer_temperature = 66
; gcode_arcs = 0
; gcode_comments = 0
; gcode_flavor = reprap
; has_heatbed = 0
; infill_acceleration = 0
; infill_first = 0
; interior_brim_width = 0
; layer_gcode =
; max_fan_speed = 100
; max_print_speed = 80
; max_volumetric_speed = 0
; min_fan_speed = 35
; min_print_speed = 10
; min_skirt_length = 0
; notes =
; nozzle_diameter = 1.25
; only_retract_when_crossing_perimeters = 1
; ooze_prevention = 0
; output_filename_format = [input_filename_base].gcode
; perimeter_acceleration = 0
; post_process =
; pressure_advance = 0
; printer_notes = ""
; resolution = 0
; retract_before_travel = 2
; retract_layer_change = 0
; retract_length = 0
; retract_length_toolchange = 10
; retract_lift = 0
; retract_lift_above = 0
; retract_lift_below = 0
; retract_restart_extra = 0
```

```
; retract_restart_extra_toolchange = 0
; retract_speed = 40
; skirt_distance = 10
; skirt_height = 1
; skirts = 0
; slowdown_below_layer_time = 5
; spiral_vase = 0
; standby_temperature_delta = -5
; start_filament_gcode = "; Filament gcode\n"
; start_gcode = G28 X0 Y0 ; home x&y axes\n
; temperature = 66
; threads = 4
; toolchange_gcode =
; travel_speed = 130
; use_firmware_retraction = 0
; use_relative_e_distances = 0
; use_volumetric_e = 0
; vibration_limit = 0
; wipe = 0
; z_offset = 0
; z_steps_per_mm = 0
; dont_support_bridges = 1
; extrusion_width = 0
; first_layer_height = 0.35
; infill_only_where_needed = 0
; interface_shells = 0
; layer_height = 0.3
; raft_layers = 0
; seam_position = nearest
; support_material = 0
; support_material_angle = 0
; support_material_buildplate_only = 0
; support_material_contact_distance = 0.2
; support_material_enforce_layers = 0
; support_material_extruder = 1
; support_material_extrusion_width = 0
; support_material_interface_extruder = 1
; support_material_interface_layers = 3
; support_material_interface_spacing = 0
; support_material_interface_speed = 100%
; support_material_pattern = pillars
; support_material_spacing = 2.5
; support_material_speed = 60
; support_material_threshold = 60%
; xy_size_compensation = 0
; bottom_infill_pattern = rectilinear
; bottom_solid_layers = 3
; bridge_flow_ratio = 1
```

```
; bridge_speed = 60
; external_perimeter_extrusion_width = 0
; external_perimeter_speed = 50%
; external_perimeters_first = 0
; extra_perimeters = 0
; fill_angle = 45
; fill_density = 40%
; fill_gaps = 1
; fill_pattern = honeycomb
; gap_fill_speed = 20
; infill_every_layers = 1
; infill_extruder = 1
; infill_extrusion_width = 0
; infill_overlap = 55%
; infill_speed = 40
; overhangs = 0
; perimeter_extruder = 1
; perimeter_extrusion_width = 0
; perimeter_speed = 40
; perimeters = 3
; small_perimeter_speed = 15
; solid_infill_below_area = 70
; solid_infill_every_layers = 0
; solid_infill_extruder = 1
; solid_infill_extrusion_width = 0
; solid_infill_speed = 20
; thin_walls = 0
; top_infill_extrusion_width = 0
; top_infill_pattern = rectilinear
; top_solid_infill_speed = 15
; top_solid_layers = 3
```